Quantifying the Role of Ocean Dynamics in Ocean Mixed Layer Temperature Variability

CASEY R. PATRIZIO[a] AND DAVID W. J. THOMPSON[a]

[a] *Department of Atmospheric Sciences, Colorado State University, Fort Collins, Colorado*

(Manuscript received 22 June 2020, in final form 21 December 2020)

ABSTRACT: Understanding the role of the ocean in climate variability requires first understanding the role of ocean dynamics in the ocean mixed layer and thus sea surface temperature variability. However, key aspects of the spatially and temporally varying contributions of ocean dynamics to such variability remain unclear. Here, the authors quantify the contributions of ocean dynamical processes to mixed layer temperature variability on monthly to multiannual time scales across the globe. To do so, they use two complementary but distinct methods: 1) a method in which ocean heat transport is estimated *directly* from a state-of-the-art ocean state estimate spanning 1992–2015 and 2) a method in which it is estimated *indirectly* from observations between 1980–2017 and the energy budget of the mixed layer. The results extend previous studies by providing quantitative estimates of the role of ocean dynamics in mixed layer temperature variability throughout the globe, across a range of time scales, in a range of available measurements, and using two different methods. Consistent with previous studies, both methods indicate that the ocean-dynamical contribution to mixed layer temperature variance is largest over western boundary currents, their eastward extensions, and regions of equatorial upwelling. In contrast to previous studies, the results suggest that ocean dynamics *reduce* the variance of Northern Hemisphere mixed layer temperatures on time scales longer than a few years. Hence, in the global mean, the fractional contribution of ocean dynamics to mixed layer temperature variability decreases at increasingly low frequencies. Differences in the magnitude of the ocean dynamical contribution based on the two methods highlight the critical need for improved and continuous observations of the ocean mixed layer.

KEYWORDS: North Atlantic Ocean; North Pacific Ocean; Atmosphere-ocean interaction; Climate variability; Interannual variability; Interdecadal variability; Oceanic variability

1. Introduction

Ocean dynamics play an essential role in governing the long-term *mean* climate. Wind-driven western boundary currents and meridional overturning circulations transport heat poleward to high latitudes where heat is released to the atmosphere (e.g., Dijkstra 2008; Hartmann 2015). The surface cooling at high latitudes promotes deep convection and mixing that links the upper ocean to the deep ocean on time scales of years to millennia (e.g., Dijkstra 2008; Pedlosky 2013). Overall, the ocean circulation accounts for nearly a third of the long-term mean meridional heat transport in the combined atmosphere–ocean system (Trenberth and Caron 2001).

The role of ocean dynamics in climate *variability* is less well understood. It is clear that they are fundamental to El Niño–Southern Oscillation (e.g., Philander 1983; Jin 1997; McPhaden et al. 2006). It is less clear whether they play a similarly important role in other aspects of climate variability, particularly at extratropical latitudes. Part of the problem lies in the relatively subtle response of the atmosphere to extratropical sea surface temperature (SST) anomalies (e.g., Kushnir et al. 2002). Another part lies in our still-evolving understanding ocean mixed layer dynamics, and thus the role of ocean dynamics in driving SST anomalies across the globe in the first place. If the SST variability over a particular region is driven predominantly by the surface heat fluxes associated with atmospheric processes, then the ocean plays a relatively passive role in climate variability (Frankignoul and Hasselmann 1977; Barsugli and Battisti 1998). But if the SST variability is also driven by ocean dynamical processes, then the ocean can play a much more active role in the climate system.

The role of ocean dynamics in mixed layer temperature variability can be conceptualized from the pedagogical models shown in Fig. 1. In all three models, we assume that variations in SSTs are linearly proportional to variations in mixed layer temperatures. In the simplest model (Fig. 1a), atmospheric temperatures T_a are driven by weather "noise" $\mathscr{F}$, and ocean mixed layer temperatures T_o are, in turn, driven by the resulting turbulent and radiative fluxes of heat at the sea surface $Q_s(\mathscr{F})$. Mixed layer temperatures are damped by the linear term $-\lambda_o T_o$, which parameterizes the damping due to the surface heat fluxes. In this model, the mixed layer integrates the input atmospheric noise $\mathscr{F}$ yielding a reddened SST response, where the reddening is a function of the heat capacity C_o and thus the depth of the mixed layer. This model is widely used as a starting point for understanding atmosphere–ocean interaction, especially in the midlatitudes (e.g., Hasselmann 1976; Frankignoul and Hasselmann 1977).

A more realistic model of the mixed layer can be formed by allowing temperatures in the atmosphere and ocean to respond to each other (Fig. 1b; Barsugli and Battisti 1998). In this case, the surface fluxes between the atmosphere and ocean respond to the temperature difference between both media $[Q_s(T_a - T_o)]$. This thermodynamic coupling between atmosphere and ocean surface temperatures results in "reduced thermal damping," which acts to redden the variance of not only sea surface temperatures but also atmospheric temperatures.

Corresponding author: Casey R. Patrizio, casey.patrizio@colostate.edu

DOI: 10.1175/JCLI-D-20-0476.1

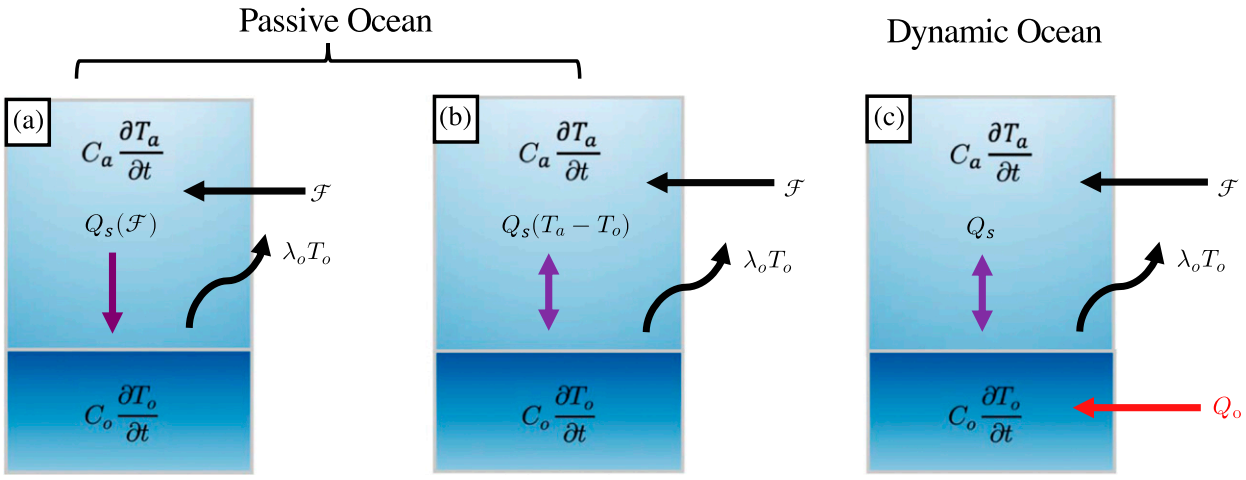

FIG. 1. Passive and dynamic ocean mixed layer models. (a) Atmospheric-noise forced ocean mixed layer (e.g., Frankignoul and Hasselmann 1977), (b) thermally coupled ocean mixed layer (e.g., Barsugli and Battisti 1998), and (c) an extension of (b) to include ocean dynamics. Here, $\mathcal{F}$ is the atmospheric heat transport, Q_s is the surface heat flux (latent, sensible and radiative), Q_o is the ocean heat transport, C_a and C_o are the heat capacities of the mixed layer and ocean, respectively, T_a and T_o are mixed layer and atmospheric temperatures, respectively, and λ_o is the mixed layer damping parameter. The models are discussed in more detail in the text.

The models shown in Figs. 1a and 1b are "passive ocean models" in that there is no explicit ocean heat transport. The models are often viewed as null hypotheses for SST variability; that is, they reflect the SST variability that would arise in the absence of ocean dynamics. Despite their simplicity, both models are able to capture aspects of observed and simulated midlatitude climate variability, such as the observed power spectrum of midlatitude SSTs (e.g., Frankignoul and Hasselmann 1977; Frankignoul 1985; Barsugli and Battisti 1998) and the covariability between the surface heat fluxes and SSTs (e.g., Cayan 1992a,b).

The models in Figs. 1a and 1b can be extended to include ocean dynamical processes by explicitly including an ocean heat transport term (Q_o in Fig. 1c). The ocean heat transport term reflects a variety of processes, including the advection of heat by the Ekman flow, large-scale geostrophic currents, eddy-induced currents, and vertical mixing at the bottom of the ocean mixed layer.

To what extent does ocean heat transport (i.e., Q_o in Fig. 1c) contribute to observed SST variability? Numerous studies have investigated this question using a variety of methods, including use of both observations and climate models. The answer depends on the location, and on the spatial and time scales of the variability. For examples: Deser et al. (2003) and de Coëtlogon and Frankignoul (2003) found that the warm-season shoaling of the mixed layer and subsequent cold-season reemergence of sequestered temperature anomalies contributes substantially to the persistence of SSTs on interannual time scales. Roberts et al. (2017) estimated the ocean heat transport as a residual in the mixed layer energy budget, and argued that ocean dynamics play an important role in driving interannual variability of upper-ocean temperatures in the equatorial oceans, the western boundary currents, and the Antarctic circumpolar current. Bishop et al. (2017) and O'Reilly and Zanna (2018) estimated the role of ocean heat transport from the lead–lag correlations between observed surface heat fluxes and SSTs across the global oceans, and reached broadly similar conclusions. Buckley et al. (2014, 2015) estimated ocean heat transport directly from an observation-assimilating ocean model and found that ocean dynamics play a dominant role in driving interannual to interdecadal variability in upper-ocean temperatures in the Gulf Stream and North Atlantic subpolar gyre. Finally, many studies have shown that mesoscale ocean dynamics play an important role in atmosphere–ocean interactions in both observations (e.g., Small et al. 2008; Frenger et al. 2013; Ma et al. 2015) and climate models (e.g., Kirtman et al. 2012; Ma et al. 2016; Siqueira and Kirtman 2016; Putrasahan et al. 2017; Saravanan and Chang 2019; Small et al. 2019, 2020).

Despite rapid improvements in our understanding of the role of ocean dynamics in SST variability, key aspects remain unclear. In large part, this is due to the difficulties inherent in observing and simulating ocean variability. Consider, for example, the cases of decadal SST variability in the North Pacific and North Atlantic Oceans. The most important pattern of decadal variability in the North Pacific sector is the so-called Pacific decadal oscillation (PDO; Mantua et al. 1997). Both atmospheric and ocean dynamical processes seemingly contribute to variability in the PDO, but their relative roles remain uncertain. Some studies have argued that the PDO is driven primarily by internal atmospheric noise and the extratropical atmospheric response to ENSO (e.g., Alexander et al. 2002; Newman et al. 2003; Deser et al. 2004). But others have argued that the PDO is also driven by ocean dynamical processes such as dynamic adjustment of the North Pacific Gyre and Kuroshio–Oyashio Extension (e.g., Latif and Barnett 1994; Schneider et al. 2002; Qiu et al. 2007; Kwon and Deser 2007; Alexander et al. 2010; Newman et al. 2016; Wills et al. 2019b) and the seasonal reemergence of North Pacific SSTs (Alexander and Deser 1995; Deser et al. 2003; Alexander et al. 2010; Newman et al. 2016)

The picture is even less clear in the case of the Atlantic multidecadal oscillation (AMO; Folland et al. 1986; Schlesinger and Ramankutty 1994). Several studies have argued that the spatial structure and time variability of the AMO are due primarily to atmospheric processes. As evidence they note that 1) the structure of the AMO can be recovered in numerical simulations run on slab-ocean models (Clement et al. 2015), 2) the lag relationships between the surface heat fluxes and SSTs associated with the AMO can be recovered in idealized models of the mixed layer that are primarily forced by stochastic atmospheric dynamics as shown in Fig. 1a (Cane et al. 2017), and 3) decadal variability in the AMO is consistent with the surface temperature response to anthropogenic aerosol loading (Booth et al. 2012; Murphy et al. 2017; Bellomo et al. 2018). However, other studies have argued that the AMO is fundamentally dependent on ocean dynamical processes. As evidence they argue that 1) in observations, the surface heat fluxes act to damp rather than drive the SST anomalies associated with the AMO (e.g., Gulev et al. 2013; O'Reilly et al. 2016; Zhang et al. 2016; Zhang 2017) and 2) in numerical models, the ocean meridional overturning circulation contributes to variations in the simulated AMO (e.g., Zhang and Wang 2013; Buckley and Marshall 2016; Delworth et al. 2017; Zhang 2017; Kim et al. 2018; Yan et al. 2018; Wills et al. 2019a; Zhang et al. 2019). Whether ocean dynamical processes contribute to SST anomalies associated with the PDO and AMO has important implications for understanding and predicting the role of both phenomena in the climate system.

The goal of this paper is to provide a comprehensive survey of the role of ocean dynamics in driving ocean mixed layer temperature variability across the globe and across a range of time scales. To do so, we use two different but complementary methods: 1) a method in which ocean heat transport is calculated *directly* from a state-of-the-art ocean state estimate, as in Buckley et al. (2014, 2015) and 2) a method in which the ocean heat transport is calculated *indirectly* from observations and the energy equation for the ocean mixed layer, as in Roberts et al. (2017). The work extends previous studies in several important ways:

- Previous work based on ocean state estimates has generally focused on select regions (e.g., Buckley et al. 2014, 2015).
- Previous work has not explicitly compared the role of ocean dynamics as inferred from observations with that derived from state estimates (e.g., Roberts et al. 2017; Small et al. 2020).
- Previous studies have frequently relied on the use of lead–lag correlations to infer causal relationships between the surface heat fluxes and SSTs (e.g., Gulev et al. 2013; O'Reilly et al. 2016; Bishop et al. 2017; O'Reilly and Zanna 2018). Here we use a diagnostic equation for the temperature variance to infer causal relationships, and highlight shortcomings of results based on lead/lag correlations.
- Previous studies have not explored the role of ocean dynamics in SST variability as a function of time scale using both observations and ocean state estimates across the global ocean. Here we exploit such analyses to reveal novel and important aspects of the role of ocean dynamics in SST variability at increasingly low-frequency time scales.

The paper is divided into four subsequent sections. The data and methods are reviewed in section 2. Results are presented in section 3. Key results and findings are discussed in section 4. Section 5 provides concluding remarks.

2. Methods and data

This section includes two parts. In section 2a we derive the equation that we use to diagnose the drivers of mixed layer temperature variance across the globe. In section 2b we describe how the equation is used to estimate ocean heat transport using two different methods: a method where ocean heat transport is estimated directly from an ocean state estimate, and a method where ocean heat transport is estimated indirectly from observed sea surface temperatures/surface heat fluxes and the energy budget of the mixed layer. Note that we do not use lead–lag correlations between the surface heat fluxes and mixed layer temperature variability to infer the role of ocean dynamics in temperature variability, as done by Gulev et al. (2013), O'Reilly et al. (2016), Bishop et al. (2017), and O'Reilly and Zanna (2018). As discussed in section 4, the use of lead–lag correlations does not unambiguously identify the role of ocean dynamics in mixed layer temperature variability.

a. *The diagnostic equation for mixed layer temperature variance*

The details of the following are provided in appendix A. Here we summarize the most salient aspects of the derivation.

The first law of thermodynamics for month-to-month temperature variability in the ocean mixed layer can be expressed as

$$\overline{C}_o \frac{\partial T'}{\partial t} = Q'_s + Q'_o, \tag{1}$$

where primes denote monthly mean anomalies; the overbar denotes the climatological mean; C_o is the heat capacity of the mixed layer; T is the monthly mean mixed layer temperature; Q_s is the net surface heat flux (i.e., the sum of the latent, sensible, and net shortwave and longwave fluxes at the surface); and Q_o is the heat flux convergence due to all ocean dynamics, including both advective processes (e.g., wind-driven Ekman flow and geostrophic currents) and diffusive processes. The climatological mean heat capacity of the mixed layer is estimated as $\overline{C}_o = \rho c_p \overline{h}$, where $\overline{h}$ is the climatological-mean mixed layer depth averaged over all months. The mean mixed layer depth is estimated from the ECCO ocean state estimate, as described in the next subsection, and is shown in Fig. 2a. Note that in the above we have neglected variations in the heat capacity. This is consistent with Roberts et al. (2017) and Buckley et al. (2014), who both used a time-invariant mixed layer depth, except that they use the maximum—rather than mean—mixed layer depth drawn from the 12-month climatology. We found that use of the maximum mixed layer depth leads to a systematic overestimate of ocean mixed heat storage when estimating the heat storage tendency in observations. It would be interesting to investigate the role of the seasonal cycle in mixed layer depths on the results in future work.

The diagnostic equation for the ocean mixed layer temperature variance is formed by squaring both sides of (1), time

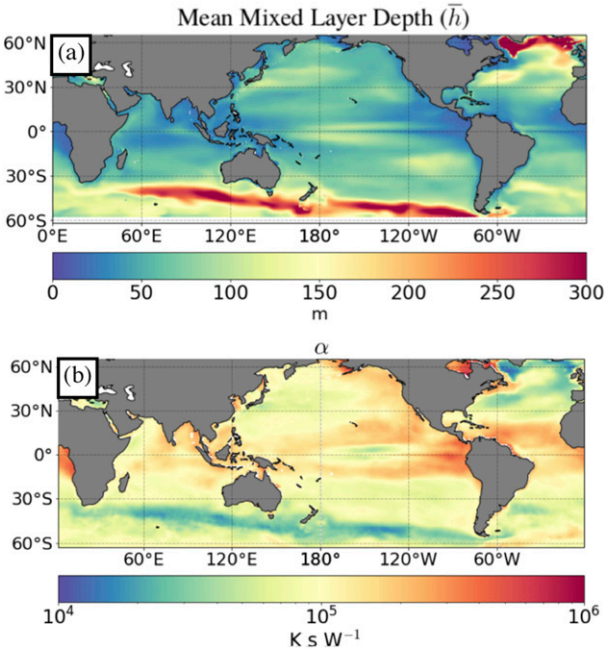

FIG. 2. (a) Climatological mean mixed layer depth $\overline{h}$ (m) from ECCO. (b) The α coefficient (K s W^{-1}) from (4) computed from ECCO mixed layer temperatures and mixed layer depths. As discussed in section 2a, α corresponds to the ability of surface heat fluxes and ocean heat transport to generate mixed layer temperature variability.

averaging, and taking the centered finite difference of the temperature tendency term so that

$$\sigma_T^2 \approx \frac{2\Delta t^2}{[\overline{C}_o^{\,2}(1-r_2)]}(\overline{Q_s'^2} + \overline{Q_o'^2} + 2\overline{Q_s'Q_o'}), \tag{2}$$

where σ_T^2 is the mixed layer temperature variance, r_2 is the mixed layer temperature lag-2 autocorrelation and Δt is the sampling time period (one month). Using (1) to substitute the temperature tendency for one $Q_s' + Q_o'$ term in (2) and defining

$$\alpha = \frac{2\Delta t^2}{[\overline{C}_o(1-r_2)]} \tag{3}$$

yields the simple diagnostic relationship

$$\sigma_T^2 \approx \tilde{Q}_s + \tilde{Q}_o, \tag{4}$$

where

$$\tilde{Q}_s = \alpha\overline{\frac{\partial T'}{\partial t}Q_s'} \tag{4a}$$

is defined as the contribution of the surface heat fluxes to the temperature variance and

$$\tilde{Q}_o = \alpha\overline{\frac{\partial T'}{\partial t}Q_o'} \tag{4b}$$

is defined as the contribution of the ocean heat transport to the temperature variance.

Note using (2) the surface heat flux and ocean dynamical contributions can also be expressed as

$$\tilde{Q}_s = \frac{\alpha}{\overline{C}_o}(\overline{Q_s'^2} + \overline{Q_s'Q_o'}), \tag{4c}$$

and

$$\tilde{Q}_o = \frac{\alpha}{\overline{C}_o}(\overline{Q_s'^2} + \overline{Q_s'Q_o'}). \tag{4d}$$

From (4a)–(4d), it is clear that the surface heat flux and ocean heat transport contributions to temperature variance can be found as either 1) the product of the temperature tendencies and the surface heat fluxes/ocean heat transport (4a) and (4b) or 2) the sum of the variances of the surface heat fluxes/ocean heat transport and their covariance (4c) and (4d). Here, the contribution of ocean dynamics (or surface heat fluxes) to the monthly mean mixed layer temperature variance at any given location is found using (4a) and (4b)—that is, by calculating the covariance between the ocean heat transport (or surface heat fluxes) and the time tendency of mixed layer temperatures, and then scaling the results by α. These equations state that ocean dynamics (or surface heat fluxes) contribute to mixed layer temperature variance in regions where the temperature tendency and ocean heat transport (or surface heat fluxes) are positively correlated. For example, if the heat transport and temperature tendency are both positive, then the diagnostic equation indicates that ocean heat transport is contributing to the temperature variance. The α coefficient, in turn, quantifies the ability of the fluxes or transport to generate temperature variance. As is evident from Figs. 2a and 2b, α is dominated by the term $\overline{C}_o^{-1}$ and thus closely resembles the spatial pattern of $\overline{h}^{-1}$. Thus covariability between the surface heat fluxes or ocean heat transport and the temperature tendency are most effective in generating mixed layer temperature variability in regions such as the subtropics and tropics where $\overline{h}$ and thus the heat capacity is small.

As summarized in appendix A, similar approaches to that outlined above were used by Yu and Boer (2006), Buckley et al. (2014) and Roberts et al. (2017) to understand the drivers of upper-ocean temperature variability.

b. *"Direct" and "indirect" methods for estimating ocean heat transport*

The contributions of the surface heat fluxes and ocean heat transport to mixed layer temperature variance (i.e., $\tilde{Q}_s$ and $\tilde{Q}_o$, respectively) are quantified from Eqs. (4a) and (4b) using two methods: 1) a method in which the ocean heat transport Q_o' is estimated directly from the ECCO ocean state estimate and 2) a method in which the ocean heat transport Q_o' is estimated indirectly from observations and the energy budget of the ocean mixed layer. In all analyses, the seasonal cycle is removed from the data by subtracting the long-term climatological means for each calendar month. All time series are detrended to minimize the effects of climate change on the results. A Butterworth filter is applied in cases where results

are calculated as a function of frequency band. In this case, the temperature and flux data are filtered before calculating all covariances.

In the case where the ocean heat transport is calculated directly, the surface heat fluxes Q'_s, ocean heat transport Q'_o, and mixed layer temperatures T' are all derived from v4r3 of the ECCO ocean state estimate (Forget et al. 2015; Fukumori et al. 2017). ECCO provides estimates of ocean heat transport, temperature and the surface fluxes for 1992–2015 at 1° horizontal resolution throughout the global ocean. In brief, the ECCO output is produced as follows [see Forget et al. (2015) and Fukumori et al. (2017) for more details]. First, a vast quantity of ocean observations is fit in a least squares sense to a state-of-the-art ocean GCM (the MITgcm). The best fit to the observations is accomplished by iteratively adjusting the model initial conditions, mixing coefficients, and surface forcings. Note that the ECCO surface fluxes are included in the adjustment. The adjusted input is then integrated forward in a free-running configuration of the MITgcm to produce the ocean state estimate. The key aspects of the ECCO output are that 1) the fitting procedure ensures that the output is consistent with the observations within their estimated uncertainties and 2) running the model in a free-running configuration ensures that the output is consistent with the laws of physics and thermodynamics, as they are represented in the numerical model. The temperature profiles used to constrain the model are sourced from gridded products (e.g., Reynolds et al. 2007), as well as a variety of in situ measurements, including from Argo floats (Argo 2000), expendable bathythermographs (XBT), and conductivity–temperature–depth (CTD) sensors.

In the case where the ocean heat transport is estimated indirectly, the surface heat fluxes and sea surface temperatures are estimated from observations, and the ocean heat transport is found as a residual in the energy budget of the ocean mixed layer [i.e., Eq. (1)]. The primary data sources are the objectively analyzed surface turbulent heat fluxes (i.e., the sum of the latent and sensible heat fluxes) from OAFlux (Yu et al. 2008), SST data from the NOAA Optimum Interpolation (OI) SST analysis produced by Reynolds et al. (2007), and surface radiative heat fluxes and wind stress from MERRA-2 reanalysis (Gelaro et al. 2017). We use the OAFlux product since it provides global coverage of the air–sea heat fluxes across multiple decades and is derived using state-of-the-art bulk flux parameterizations (Yu et al. 2008). All data are applied over the period 1980–2017 and at 1° resolution. For brevity we refer to the combined OAFlux/NOAA OI SST/MERRA-2 data as the "OAFlux" dataset throughout the rest of the paper, although it should be understood that radiative fluxes are from MERRA-2. We also tested the robustness of select OAFlux results to the use of different atmospheric reanalyses, including MERRA-2, ERA5 (Hersbach and Dee 2016), and the NOAA–CIRES–DOE Twentieth Century Reanalysis, version 3 (Slivinski et al. 2019).

Note that indirect estimates of ocean heat transport are inevitably influenced by biases in the SST and surface heat flux data (e.g., Hall and Bryden 1982; Talley 1984; Bryden and Imawaki 2001). The uncertainties in the OAFlux air–sea heat fluxes due to biases in the various input data are provided in the OAFlux product. The contributions of observational error to uncertainties in the mixed layer temperature variance [i.e., uncertainty in Eqs. (4c) and (4d)] is reviewed in appendix A.

The equations used to estimate ocean heat transport and temperature variance [Eqs. (1)–(4)] are based on mixed layer temperatures, but we use observations of sea surface temperatures since mixed layer temperatures are not as widely available. Sea surface and mixed layer temperatures are linearly related to each other but have different amplitudes. For example, Fig. 3a shows the SST variances σ^2_{SST} from the NOAA OI product and Fig. 3b the mixed layer temperature variances σ^2_T from ECCO. The patterns of the variances are nearly identical, with maxima in the western boundary currents and the equatorial Pacific. However, as shown in Fig. 3d, the amplitudes are very different, with larger SST variances found at subtropical and extratropical latitudes but larger mixed layer temperature variances found in the deep tropics. Note that a very similar pattern of variance ratios arises between mixed layer and sea surface temperatures derived from ECCO (3e), which reveals that the differences in Fig. 3d are not solely a result of differences between the ECCO SST and NOAA SST.

From Fig. 3d, it is clear that using SSTs rather than mixed layer temperatures in Eq. (1) would systematically overestimate the importance of ocean heat transport in the extratropics but underestimate it in the tropics. To avoid this bias, we linearly scale the observed SST tendencies by the square root of the ratio of the 1) ECCO mixed layer temperature variance to 2) the ECCO SST variance. That is, we estimate the observed mixed layer temperature tendencies for Eq. (1) as

$$\frac{\partial T}{\partial t} = \sqrt{\frac{\sigma^2_{T,\mathrm{ECCO}}}{\sigma^2_{\mathrm{SST,ECCO}}}}\frac{\partial \mathrm{SST}}{\partial t}, \tag{5}$$

where T denotes mixed layer temperatures. The above scaling provides an estimate of the "observed" mixed layer temperature tendencies that 1) are perfectly correlated with the observed SST tendencies and 2) preserve the ratio of SST variances to mixed layer temperature variances found in ECCO. Figure 3c shows the resulting "observed" mixed layer temperature variances and Fig. 3f shows the corresponding (log) ratio of the observed to ECCO mixed layer temperature variances. The differences between the OAFlux estimate of σ^2_T and the ECCO σ^2_T are generally small.

Select results are reproduced using mixed layer temperatures derived from version 4.1.1 of the Met Office Hadley Centre gridded analyses of in situ ocean temperature profiles (EN4; Good et al. 2013). The main sources for EN4 analyzed temperature profiles are the World Ocean Database (WOD09; Boyer et al. 2009), the Global Temperature and Salinity Profile Program (GTSPP) (U.S. National Oceanographic Data Center 2006), and Argo floats. The EN4 temperature profiles provide an additional residual estimate of ocean heat transport based on observed mixed layer rather than sea surface temperatures.

3. Results

a. *Diagnosis of monthly mean mixed layer temperature variability*

Figures 4a and 4b show the variances of ocean mixed layer temperatures from the observations (left) and ECCO output

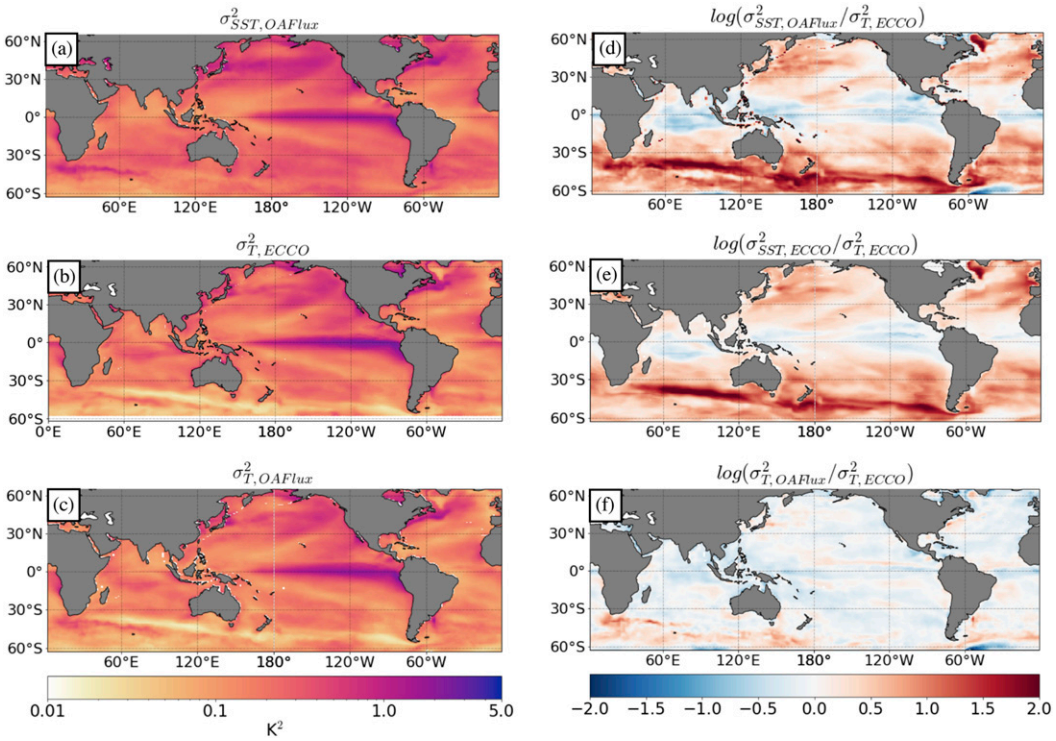

FIG. 3. (a) Monthly SST variance (K^2) from OAFlux. (b) Monthly mixed layer temperature variance (K^2) from ECCO. (c) OAFlux estimate of monthly mixed layer temperature variance (K^2) from Eq. (5). (d) Log ratio of the OAFlux monthly SST variance to the ECCO monthly mixed layer temperature variance. (e) Log ratio of the ECCO monthly SST variance to the ECCO monthly mixed layer temperature variance (K^2). (f) Log ratio of the OAFlux estimate of monthly mixed layer temperature variance to the ECCO monthly mixed layer temperature variance (K^2).

(right). Recall that the observed mixed layer temperature variances are derived from observed SSTs using Eq. (5). Figures 4c–f show the associated contributions of ocean dynamics and the surface heat fluxes to the temperature variances ($\tilde{Q}_o$ and $\tilde{Q}_s$). As a check on the analyses, we confirmed that the sums of $\tilde{Q}_s$ and $\tilde{Q}_o$ are equal to the total variances in the top row (not shown). Figures 5a–d show the same results as Figs. 4c–f, but here the ocean dynamical and surface heat flux contributions are shown as a fraction of the total temperature variances. Recall that 1) the ocean dynamical contributions include heat transport by both advection and diffusion and 2) the surface fluxes are a combination of the radiative fluxes and the turbulent fluxes of latent and sensible heat. The decomposition of the ocean dynamical contributions into its various components is discussed further below.

The ocean dynamical contributions to mixed layer temperature variance provided by the observations and ECCO exhibit similar patterns but different amplitudes (Figs. 4c,d). Both methods indicate that ocean dynamics contribute most to mixed layer temperature variance in the vicinity of the Kuroshio–Oyashio and its downstream extension; the Gulf Stream and its downstream extension; the Agulhas Current; the Malvinas Current; and in various regions throughout the tropics, including the eastern tropical Pacific cold tongue and the equatorial Atlantic. The most pronounced differences between the methods are found in the extratropics, where the observational estimates of the ocean dynamical contributions are nearly twice as large as the ECCO-based estimates. The differences are even more clear when the ocean dynamical contributions are shown as a fraction of the total variances in mixed layer temperatures (Figs. 5a,b).

The surface heat flux contributions provided by the observations and ECCO likewise exhibit similar spatial patterns but different amplitudes (Figs. 4e,f). Both methods indicate that the surface fluxes act to drive SST variability (i.e., they are positive) everywhere except in the equatorial cold tongue regions, where they act to damp SST variability. Both observations and ECCO also indicate maxima in $\tilde{Q}_s$ in the subtropics, which are most clear when $\tilde{Q}_s$ is scaled by the total temperature variances (Figs. 5c,d). The subtropical maxima are consistent with large variability in the latent heat fluxes at subtropical latitudes (e.g., Chiang and Vimont 2004; Xie and Carton 2004; Amaya et al. 2017). As anticipated, the most pronounced differences between the observational and ECCO-based results are again found in the extratropics, where the ECCO-based estimates of $\tilde{Q}_s$ are roughly twice as large as the observational-based estimates (Figs. 5c,d). Note that in general the surface flux results in Fig. 5 are dominated by the turbulent fluxes of latent and sensible heat, and that the radiative fluxes play a relatively small role (not shown).

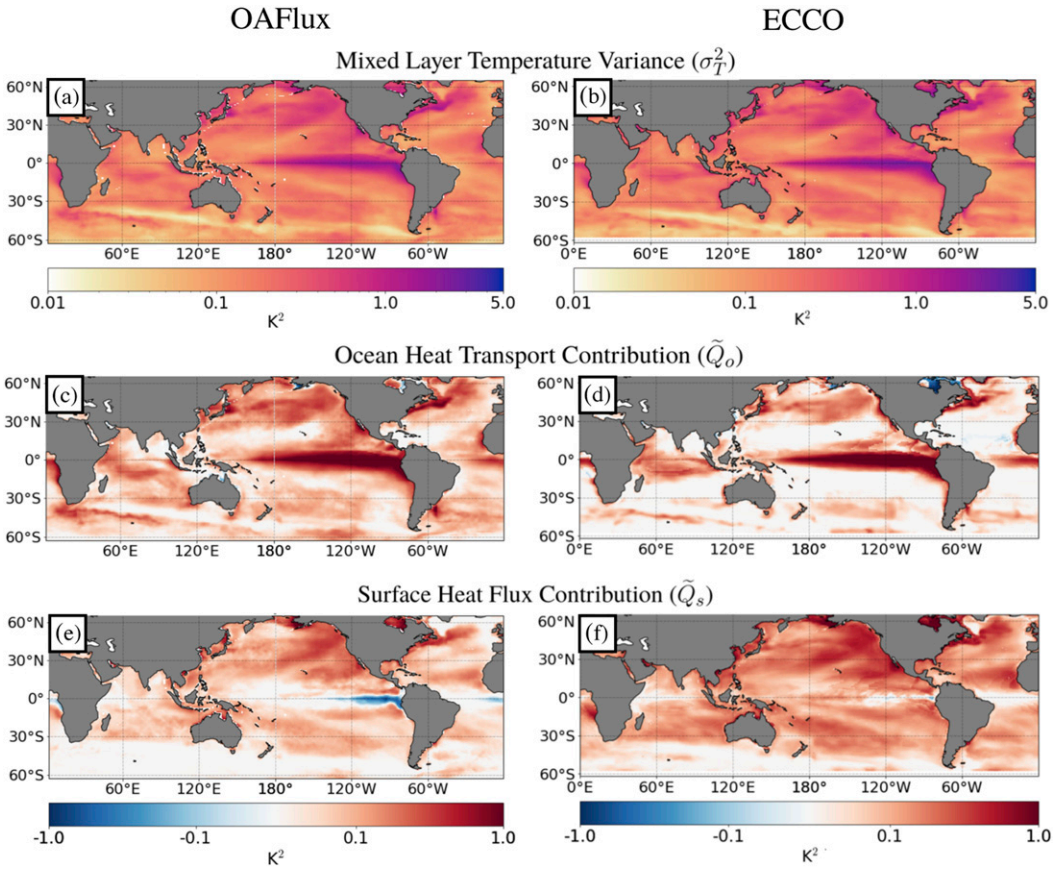

FIG. 4. (a),(b) Monthly mixed layer temperature variance σ_T^2 (K^2) from OAFlux and ECCO, respectively. As discussed in section 2b, the OAFlux mixed layer temperature variance is estimated from Eq. (5). (c),(d) Ocean heat transport contribution to mixed layer temperature variance $\tilde{Q}_o$ (K^2) derived from the indirect method using OAFlux and the direct method using ECCO. (e),(f) Surface heat flux contribution to mixed layer temperature variance $\tilde{Q}_s$ (K^2) for OAFlux and ECCO.

The relative importance of the surface heat fluxes and ocean heat transport for mixed layer temperature variability is summarized in Figs. 5e and 5f, which show the differences in the fractional contributions from the top panels. Warm colors indicate regions where the surface heat fluxes account for a larger fraction of the mixed layer temperature variance than ocean dynamics, and vice versa. Both the observational and ECCO-based results indicate that ocean heat transport dominates mixed layer temperature variability in the tropical oceans (blue shading in Figs. 5e and 5f). But as noted above, the two methods differ widely in the extratropics. The observations suggest that ocean dynamics account for a slightly larger fraction of the temperature variance than the surface heat fluxes over most of the extratropics (Fig. 5e). In contrast, the ECCO-based results suggest that the surface heat fluxes account for the predominance of the temperature variance at extratropical latitudes (Fig. 5f), with notable exceptions found in major current regions such as the Kuroshio, Gulf Stream, Agulhas Current, Malvinas Current, and Antarctic Circumpolar Current.

Figures 6 and 7 explore the decomposition of the total ocean heat transport contributions into various physical processes. The top row in Fig. 6 shows the total ocean dynamical contributions reproduced from Figs. 4c and 4d. Subsequent rows show the contributions from the horizontal Ekman heat transport computed using the surface wind stresses from MERRA-2 (Fig. 6c) and ECCO (Fig. 6d), and the residuals due to all other ocean dynamical processes, found as the differences between the top and middle panels (Figs. 6e,f). Figure 7 shows a different decomposition of the ocean dynamical contributions based on the ECCO estimates of diffusive and advective heat transport. Here the top panel shows the total ocean dynamical contributions from ECCO (reproduced from Fig. 4d). But now the middle panel shows the components due to diffusive mixing (Fig. 7b) and the bottom panel the components due to advective heat transport (Fig. 7c). Note that Fig. 7b includes mixing due to convective processes and parameterized isopycnal diffusion (Redi 1982; Gaspar et al. 1990), whereas Fig. 7c includes advective heat transport due to explicitly resolved large-scale currents and eddy-induced transport as parameterized by the Gent and McWilliams (1990) scheme.

The observational and ECCO-based estimates of horizontal Ekman heat transport are nearly identical (Figs. 6c,d). Hence,

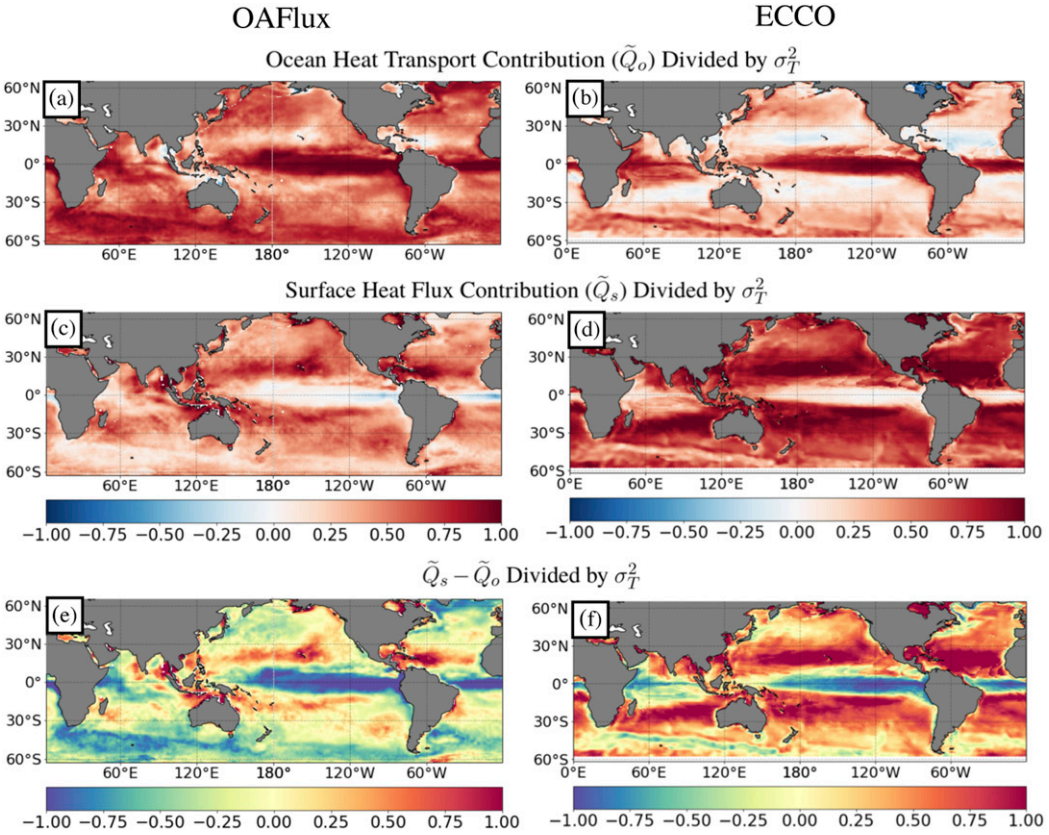

FIG. 5. (a)–(d) As in Figs. 4c–e, except results are divided by the mixed layer temperature variance σ_T^2. (e),(f) The difference between the surface heat flux contribution and the ocean heat transport contribution $\tilde{Q}_s - \tilde{Q}_o$ divided by the mixed layer temperature variance using the indirect method (OAFlux) and the direct method (ECCO). Warm colors: surface heat flux contribution is dominant; cool colors: ocean heat transport contribution is dominant.

the resulting residual contributions from all other ocean dynamical processes differ greatly between the two methods (Figs. 6e,f). As such, the horizontal Ekman heat transport accounts for roughly half of the total ocean dynamical contributions to mixed layer temperature variability in the ECCO product, but a much smaller fraction of the total ocean dynamical contributions in the observations. Additionally, the differences in the total ocean dynamical contributions to SST variability shown in Figs. 6a and 6b arise almost entirely from non-Ekman processes. As evidenced in Fig. 7, diffusive processes account for a very small fraction of the temperature variance on monthly mean time scales. However, as shown in the next section, diffusive processes play a more important role on lower-frequency time scales.

The results in Figs. 4–7 provide novel and comprehensive estimates of the ocean dynamical contributions to mixed layer temperature variability. They are broadly consistent with results shown in recent studies (e.g., Bishop et al. 2017; Roberts et al. 2017; Small et al. 2020), and indicate that ocean dynamics play an important role in monthly mean mixed layer temperature variability in equatorial regions and in the vicinity of the major extratropical boundary currents. However, the results also reveal important inconsistencies in the ocean dynamical contributions estimated from observations and the ECCO product. In general, the observations suggest a much larger role for ocean dynamical processes in SST variability than the ECCO output does. The inconsistencies have potentially important implications for our understanding of the role of the ocean in extratropical climate variability.

It is unclear why the observations suggest a larger role for ocean dynamical processes. One possible explanation is that the 1° ECCO product used here underestimates the role of mesoscale ocean dynamics in driving mixed layer temperature variability. Mesoscale ocean processes play an important role in facilitating atmosphere–ocean interactions (Ma et al. 2016; Siqueira and Kirtman 2016; Saravanan and Chang 2019; Small et al. 2019, 2020) and substantial differences in vertical and horizontal ocean heat transports arise in simulations with fine (~0.1°) ocean resolution relative to more coarse (~1°) resolution (Griffies et al. 2015). It would be interesting to assess higher-resolution ocean state estimates using the methods described in this paper in future work.

b. *Time scale dependence*

Here we explore the contributions of ocean dynamics to mixed layer temperature variance in data that have been

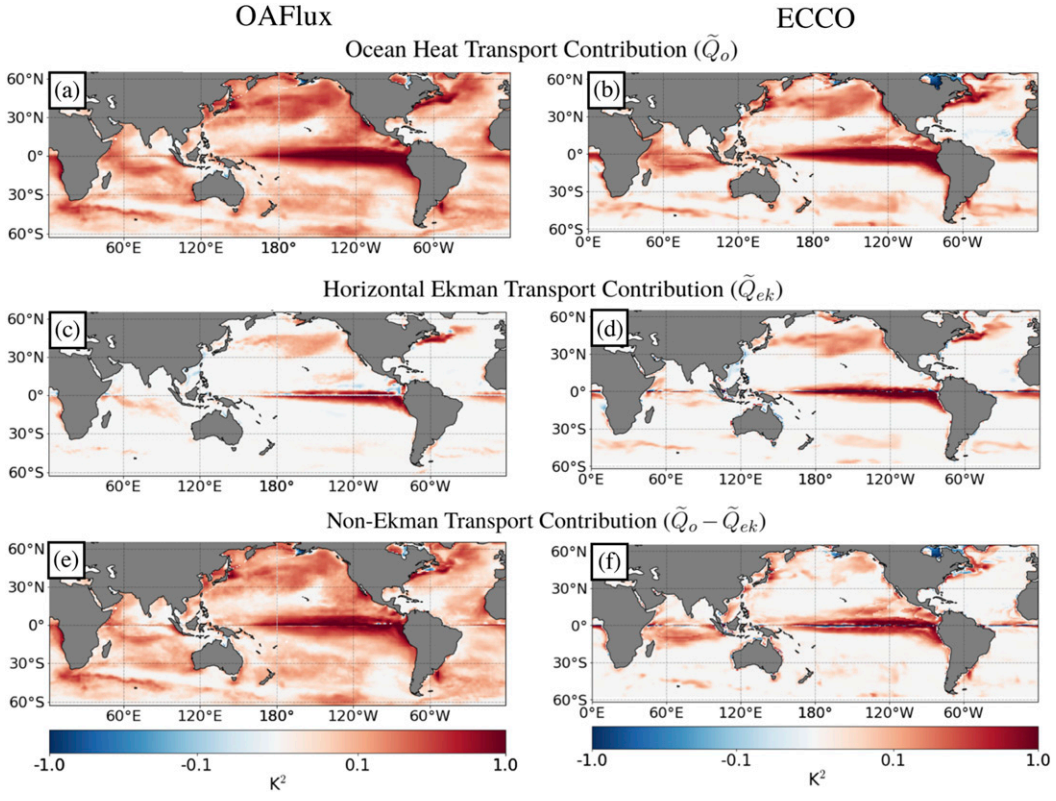

FIG. 6. (a),(b) Ocean heat transport contribution to mixed layer temperature variance $\tilde{Q}_o$ (K^2) derived from the indirect method using OAFlux and the direct method using ECCO, respectively. (c),(d) Horizontal Ekman transport contribution to mixed layer temperature variance $\tilde{Q}_{ek}$ (K^2), calculated using surface wind stress from MERRA-2 reanalysis in (c) and surface wind stress from ECCO in (d). (e),(f) Non-Ekman transport contribution to mixed layer temperature variance $\tilde{Q}_o - \tilde{Q}_{ek}$ (K^2), calculated as the difference between the top and middle panels for OAFlux and ECCO, respectively.

low-pass filtered with a Butterworth recursive filter. Note that the temperature and flux data are filtered before calculating the covariances in Eq. (4). We first explore the spatial patterns of 4-yr low-pass filtered variability. We then explore the sensitivity of the results to different filter cutoffs. As done above for unfiltered data, we confirmed that the sums of $\tilde{Q}_s$ and $\tilde{Q}_o$ are equal to the total variances in all low-pass filtered results (not shown).

Figures 8a and 8b show the 4-yr low-pass filtered mixed layer temperature variances from the observations and ECCO products. In general, the low-pass filtered variances are very similar to their unfiltered counterparts, albeit with small amplitudes (cf. Figs. 4a,b and 8a,b). Both exhibit centers of action in the eastern tropical Pacific, the extratropical North Pacific, and the vicinity of the Gulf Stream and its extension. In contrast, the contributions of ocean dynamics to the temperature variances (Figs. 8c,d) are dramatically different between the low-pass filtered and unfiltered data, particularly in the Northern Hemisphere. Ocean dynamics act to enhance mixed layer temperature variability throughout the NH when all time scales are included in the analysis (Figs. 4c,d). In contrast, the ocean dynamics appear to oppose mixed layer temperature variance in regions throughout the North Pacific and in the Gulf Stream Extension region of the North Atlantic on time scales longer than 4 years (Figs. 8c,d). The result is reproducible in both the observations and ECCO output. Thus the discrepancies between the observed and ECCO-derived estimates of $\tilde{Q}_o$ highlighted in Fig. 4 are primarily due to ocean dynamics on time scales between one month and four years.

The apparent suppression of multiannual mixed layer temperature variance by ocean dynamics in the North Pacific and North Atlantic is surprising. Ocean dynamics are generally believed to play an increasingly important role in SST variability on low-frequency time scales (e.g., Bjerknes 1964; Gulev et al. 2013; Buckley et al. 2014; O'Reilly et al. 2016). Decadal SST variability in the North Pacific has been frequently linked to dynamic adjustments of the North Pacific Gyre and Kuroshio–Oyashio Extension that occur via oceanic Rossby wave propagation (e.g., Latif and Barnett 1994; Kwon and Deser 2007; Wills et al. 2019b). Also, previous studies have linked multidecadal SST variability in the North Atlantic to variations in the Atlantic meridional overturning circulation (e.g., Buckley and

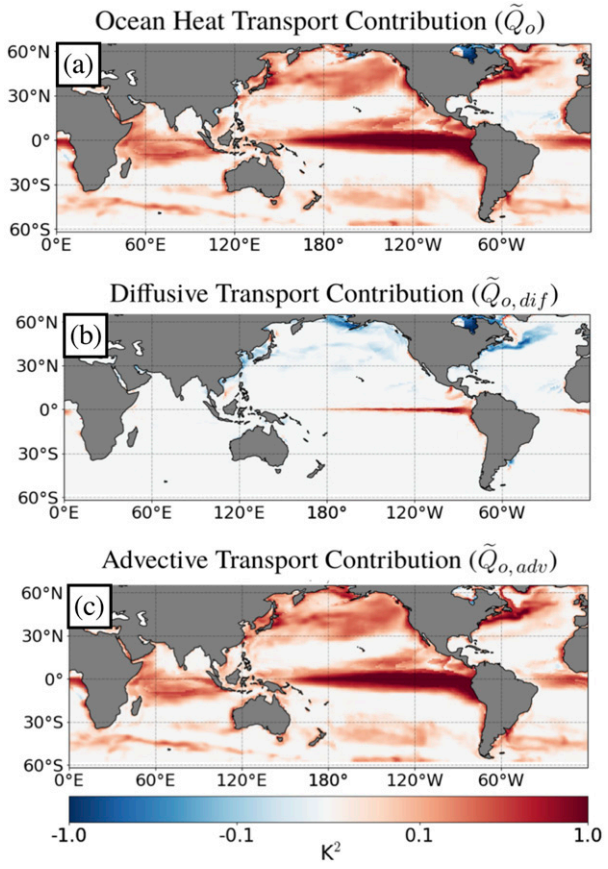

FIG. 7. (a) Ocean heat transport contribution to mixed layer temperature variance from ECCO (repeated from Fig. 6b). (b),(c) The components of the contribution due to diffusive heat transport $\tilde{Q}_{o,\mathrm{dif}}$ (K^2) and advective heat transport $Q_{o,\mathrm{adv}}$ (K^2).

Marshall 2016; Kim et al. 2018; Yan et al. 2018; Zhang et al. 2019). It is possible that ocean dynamics play an important role on time scales longer than those that can be resolved in the relatively short records afforded by the ECCO and OAFlux products (1992–2015 and 1980–2017, respectively). However, the results in Fig. 8 suggest that—on the time scales resolvable in the analysis—multiannual mixed layer temperature variability in both the North Pacific and North Atlantic is generally damped by ocean dynamics.

Why do ocean dynamics suppress mixed layer temperature variance on multiannual time scales? As discussed above, the ocean dynamical contributions to mixed layer temperature variability arise from advective heat transport and diffusion by convective and parameterized isopycnal mixing at the base of the mixed layer. Figure 9 shows the advective and diffusive contributions for 4-yr low-pass filtered data. The key result in Fig. 9 is that while convective and parameterized isopycnal mixing play a very small role in the unfiltered data (Fig. 7b), they play a prominent role on low-frequency time scales (Fig. 9b). Hence the results suggest that the role of diffusive mixing overwhelms the role of advection in mixed layer temperature variability on time scales longer than a few years in the extratropical northern oceans.

To more clearly illustrate the time scale dependency of the results, Fig. 10 explores the contributions of the surface heat fluxes and ocean heat transport to SST variability as a function of low-pass filter length. Results are shown for variances averaged over the globe, the extratropical NH and SH, and the tropics (note that the results show the spatial averages of the variances, not the variances of the spatial averages). The top half of the plot (marked OAFlux) indicates results derived from the observations over the period 1980–2017: the first row shows the total area-averaged mixed layer temperature variance (black), the contributions to temperature variance due to ocean dynamics (blue), and the contributions to temperature variance due to surface fluxes (green); the second row shows the fractional rather than total contributions due to ocean dynamics (blue shading) and surface fluxes (green shading). The uncertainties in the variance estimates due to uncertainties in the observations are indicated by the transparent colored shadings in the top row (see appendix A for details of the uncertainty analysis). The bottom half of the plot (marked ECCO) shows the same results, but calculated for ECCO over the ECCO period of record 1992–2015. The figure highlights three key results:

1) As expected, temperature variances—and thus the ocean dynamical and heat flux contributions to temperature variances—decrease as the filter length is increased.
2) The contributions of ocean dynamics to the mixed layer temperature variances are roughly twice as large in observations as they are in ECCO output at all time scales. In the case of unfiltered data (i.e., filter length 0), the observations suggest that ocean dynamics account for ~55% of unfiltered mixed layer temperature variability averaged over the extratropical Northern Hemisphere, ~65% averaged over the extratropical Southern Hemisphere, and ~65% averaged over the globe. In contrast, in the ECCO output, ocean dynamics account for only ~30%, ~35%, and ~45% averaged over the same respective domains. The differences between the unfiltered OAFlux and ECCO results are not explained by uncertainties in the OAFlux estimates (transparent shading in the top row). They are also reproducible when the OAFlux results are computed for the ECCO period of record (not shown).
3) Both the observations and ECCO indicate that the fractional contribution of ocean dynamics to NH mixed layer temperature variability decreases at increasingly low frequencies (blue shading in Figs. 10b and 10f). In fact, the contribution of ocean dynamics to NH temperature variance is negative at filter lengths longer than ~3 years (blue lines in Figs. 10b and 10f). The striking differences between the contributions of the surface fluxes and ocean dynamics far exceed the uncertainties in the OAFlux estimates (green and blue transparent shading in Fig. 10b, top). We repeated the analysis shown in Fig. 10 for the extratropical North Pacific and North Atlantic basins separately (see Figs. B1a,f and B2a,f in appendix B). Both datasets indicate that ocean dynamics play a vanishingly small role in driving SST

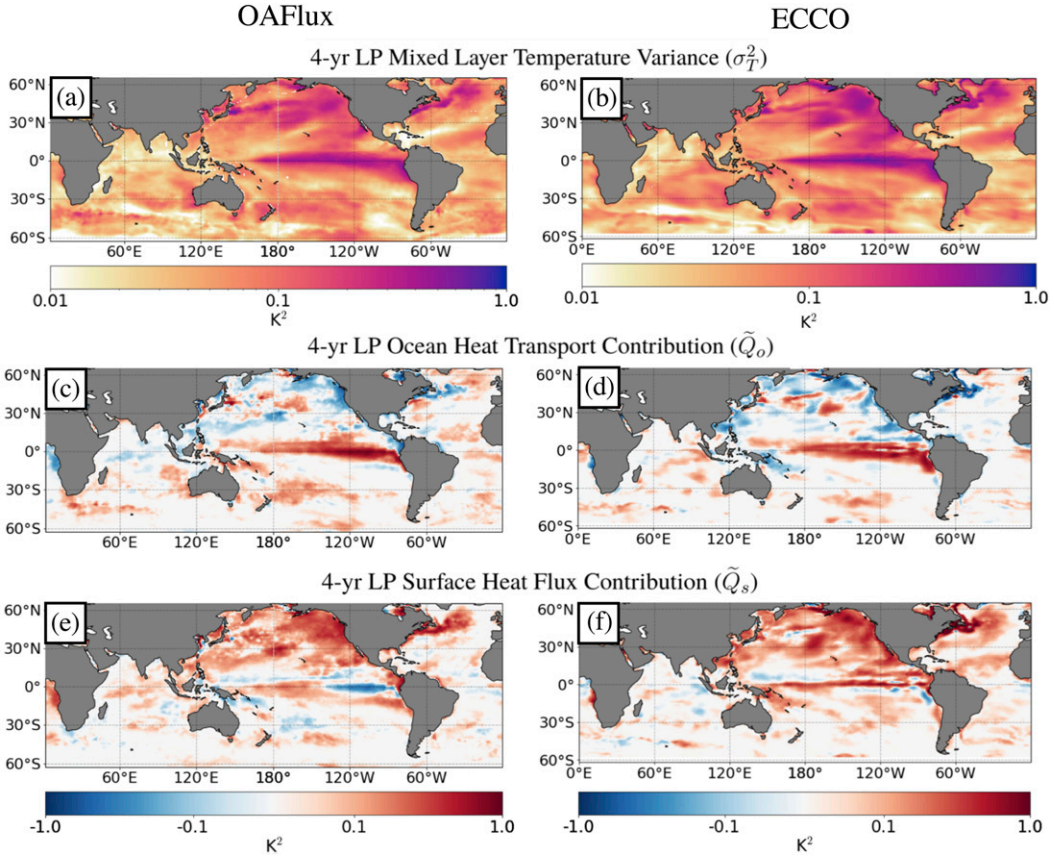

FIG. 8. As in Fig. 4, but for 4-yr low-pass (LP) filtered data.

variability in both basins on time scales longer than ~4 years (Figs. B1a,f and B2a,f) and that the results are robust to the uncertainty estimates provided in the OAFlux product (transparent shading in Figs. B1a and B2a). Both datasets also indicate that the ocean dynamical contributions are weakly negative (i.e., that they suppress SST variance–at frequencies longer than a few years in the North Pacific; Figs. B1a,f). Only ECCO indicates that the ocean dynamical contributions are negative in the North Atlantic (Figs. B2a,f). The signature of increasingly small fractional contributions of ocean dynamics at increasingly low frequencies is less pronounced in the tropics or Southern Hemisphere (Figs. 10c,d,g,h) but is apparent in the global mean (Figs. 10a,e).

Clearly, the vanishingly small contribution of ocean dynamics to multiannual mixed layer temperature variability in the Northern Hemisphere has important implications for understanding the drivers of North Pacific and North Atlantic climate variability. Figure 11 tests the reproducibility of this key result in four other data sources: output from the MERRA-2 and ERA5 reanalysis products (Figs. 11a,b), output from the NOAA–CIRES–DOE Twentieth Century Reanalysis (20CR; Fig. 11c), and a combination of the OAFlux fluxes with mixed layer temperature tendencies from EN4 (Fig. 11d). All results are based on the 1980–2017 period to facilitate comparison with the observational (OAFlux) results shown in Fig. 10. Figure 11 shows results integrated over the Northern Hemisphere; Figs. B1b–d and B2b–d show results integrated over the North Atlantic and Pacific basins, separately. Note that the analysis of the combined EN4–OAFlux data allows us to better understand how the observational results depend on the scaling used to convert SST to mixed layer temperature variances [Eq. (5)].

As evidenced in Fig. 11, the increasingly small fractional contributions of ocean dynamics to low-frequency Northern Hemisphere mixed layer temperature variability is reproducible in all datasets considered in the figure. The contributions are negative, indicating that ocean dynamics are suppressing low-frequency temperature variance, in all data sources except for mixed layer temperatures derived from EN4. But even in this case, the fractional contribution of ocean dynamics to the temperature variance is considerably less than that associated with the surface heat fluxes, albeit the uncertainties in the EN4 estimates calculated using the formulation in appendix A are large on time scales longer than a few years. Note that output from all the observational data sources indicates a larger role for ocean dynamics in unfiltered data than output from ECCO (roughly 60% for observations versus 30% for ECCO). Thus, the differences in $\tilde{Q}_o$ between the indirect method and direct method are not due to the SST-tendency scaling given in Eq. (5).

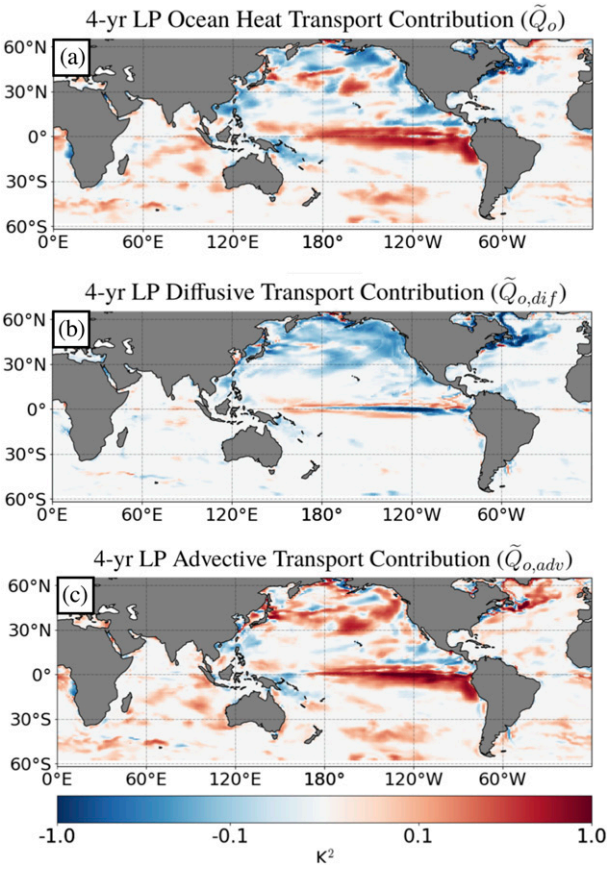

FIG. 9. (a)–(c) As in Figs. 7a–c, but for 4-yr low-pass (LP) filtered data.

The observational results in Figs. 10 and 11 are based on the period of record following 1980. That is because remotely sensed data are widely available from the late 1970s, and thus major reanalyses such as ERA5 and MERRA2 are only available after 1979. However, the 20CR product is available extending back to 1836. We reproduced the results in Fig. 11c using the 20CR product over periods of record extending from 1950–2017 and 1900–2017 (not shown). As in Fig. 11c, the ocean dynamical contributions to mixed layer temperature variability decrease more rapidly than the surface heat flux contributions at increasingly low frequencies. Unlike Fig. 11c, the ocean dynamical contributions do not become negative at low frequencies. However, the SST and flux measurement data are relatively sparse and exhibit more notable biases during the early and middle twentieth century (e.g., Kent et al. 2017; Davis et al. 2019, and references therein). Thus we view estimates of ocean dynamics for the early and middle twentieth century as much more uncertain than estimates for the last few decades.

4. Discussion

The results in the previous section highlight two surprising results: 1) The fractional contribution of ocean dynamics to NH-mean and global-mean mixed layer temperature variability deceases as the time scale increases, and 2) over certain areas of the extratropical North Atlantic and North Pacific, ocean dynamics act to *reduce* rather than increase the temperature variance on multiannual time scales. The results emerge from analyses of the temperature variance budget, as summarized in section 2. And they are reproducible in estimates of ocean heat transport derived both indirectly from observations of surface heat fluxes and SSTs, and directly using the ECCO ocean state estimate. However, they also contradict previous findings in which the role of ocean dynamics in SST variability is inferred from lag correlations between the surface heat fluxes and SSTs. Here we comment on the differences and similarities between the methods used here and in previous analyses.

Numerous studies have used lag correlations between SSTs and the surface heat fluxes to infer the role of ocean dynamics in SST variability (e.g., Gulev et al. 2013; O'Reilly et al. 2016; Bishop et al. 2017; Zhang 2017; O'Reilly and Zanna 2018). The reasoning is as follows: If the surface heat fluxes Q_s (defined positive down) are positively correlated with SSTs when leading the SST field, then the surface heat fluxes enhance temperature anomalies. Conversely, if the fluxes Q_s are negatively correlated with SSTs when leading the SST field, then the surface heat fluxes damp SST anomalies and thus the temperature anomalies must be driven by ocean heat transport. On the basis of this logic, previous studies have interpreted positive correlations between Q_s and increasing SSTs on monthly and annual time scales as evidence that the surface heat fluxes are driving high-frequency SST variability. Likewise, they have interpreted negative correlations between Q_s and increasing SSTs on multiannual to multidecadal time scales as evidence that ocean dynamics are driving low-frequency SST variability (e.g., Gulev et al. 2013; O'Reilly et al. 2016; Bishop et al. 2017; Zhang 2017; O'Reilly and Zanna 2018).

However, as also emphasized in Cane et al. (2017), the sign of the lag correlation between SSTs and the surface heat fluxes does not unequivocally identify the role of ocean dynamics. Consider the North Atlantic as an example. Our results suggest that ocean dynamics play a fractionally smaller role in driving SST variability as the time scale of the variability increases, with ocean dynamics suppressing SST variability over the Gulf Stream region on time scales longer than ~4 years (Figs. 8c,d). In contrast, Gulev et al. (2013), O'Reilly et al. (2016) and others have used lead–lag correlations between SSTs and the surface heat fluxes to argue that ocean dynamics must play a key role in driving North Atlantic SST variability at low frequencies.

Figures 12 and 13 make clear how our results relate to those in previous studies, and highlight the shortcomings of using lag correlations between the surface heat fluxes and the SSTs to infer the role of ocean dynamics. The left column in Fig. 12 is derived from the left column of Fig. 4 but is focused on the North Atlantic. The top panel shows the total variance in mixed layer temperatures, the middle the contributions of ocean dynamics, and the bottom the contributions of the surface heat fluxes. All results are derived from the indirect method with OAFlux data. The right column is similar to the

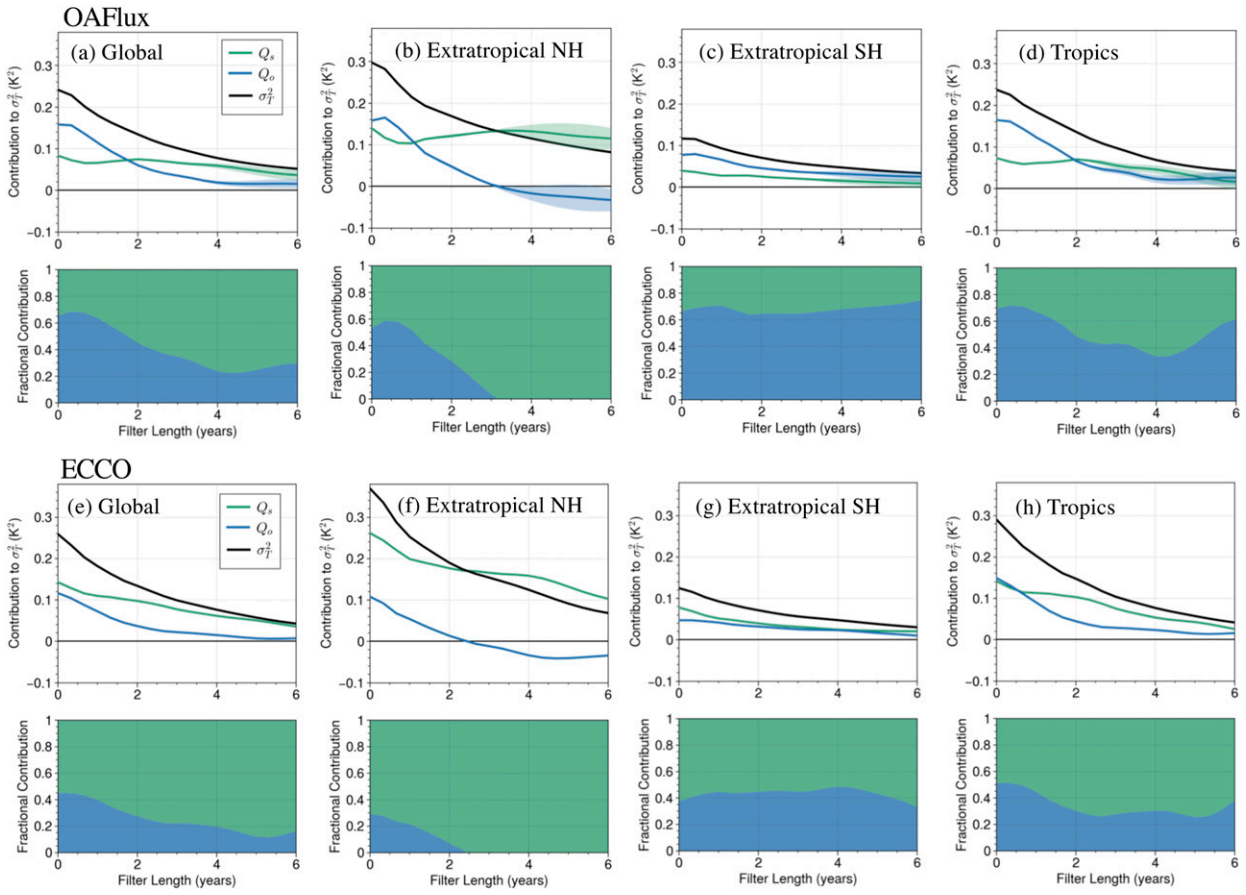

FIG. 10. Spatially averaged contributions of ocean dynamics (blue) and surface heat fluxes (green) to mixed layer temperature variance (black). Results are shown as a function of low-pass filter length, as indicated on the horizontal axis. (a)–(d) Results for the observations based on OAFlux. (e)–(h) Results based on ECCO. The domains are the global oceans (60°S–60°N), the extratropical Northern Hemisphere (NH; 30°–60°N), the extratropical Southern Hemisphere (SH; 30°–60°S), and the tropics (30°S–30°N) The line plots on the top panels indicate the total contributions (K^2), and OAFlux uncertainty is shown as transparent shading. The solid shading on the bottom panels indicates the fractional contributions.

left column of Fig. 8, and shows the respective results for 5-yr low-pass filtered data. As discussed earlier in the text, ocean heat transport contributes substantially to temperature variance in the Gulf Stream Extension region in the unfiltered data (Fig. 12b) but acts to decrease temperature variance in the Gulf Stream region at lower frequencies (Fig. 12e).

Figure 13 shows the lead/lag correlations between SSTs and the surface heat fluxes (top) and ocean heat transport (bottom) averaged over the Gulf Stream Extension region (as indicated by the dashed boxes in Fig. 12). Negative lags denote that the fluxes or transport lead the SST field. The sign of the heat fluxes and ocean heat transport is positive into the local ocean mixed layer. To facilitate comparison between the lag-correlation method and the method outlined in section 2, the contributions of the surface heat fluxes and ocean dynamics to the temperature variance (i.e., $\tilde{Q}_s$ and $\tilde{Q}_o$, respectively) averaged over this region are indicated in the bottom left of each panel. Note that the results in the bottom panels (Figs. 13b,d) are comparable to Figs. 2a and 2b from O'Reilly et al. (2016).

Starting with the unfiltered results (left column): The correlations between Q_s and the SSTs are positive when the fluxes lead SSTs and negative when the fluxes lag SSTs (Fig. 13a; recall that Q_s is positive down). According to the logic discussed previously, this suggests that Q_s enhances SST anomalies and hence contributes to SST variability. In this case, inferences based on lag correlations are consistent with the results derived from our Eq. (4). In particular, Eq. (4a) states that the contribution of Q_s to temperature variability is given by the covariance between Q_s and the SST tendency, which relates to the *change* in the correlation across lag zero. This can be clearly seen by expanding the temperature tendency in the following:

$$\widetilde{Q_s} = \overline{Q_s' \frac{\partial T'}{\partial t}} \approx \overline{Q_s'(t) T'(t+\Delta t)} - \overline{Q_s'(t)' T'(t-\Delta t)}. \qquad (6)$$

The first term on the RHS of (6) relates to the correlation at negative lags (i.e., Q_s *leads* SST), and the second term relates to

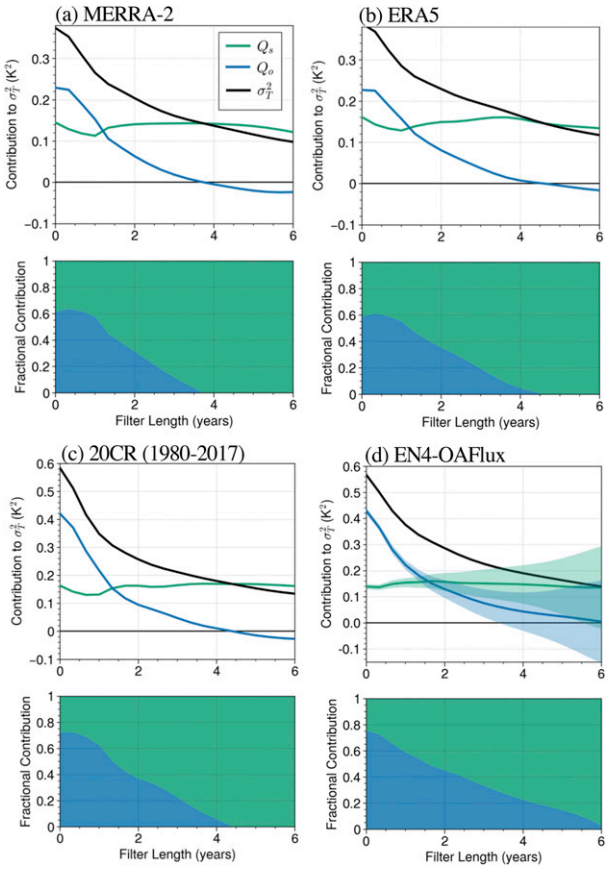

FIG. 11. As in Figs. 10b and 10f, but for output from (a) MERRA-2, (b) ERA5, (c) the NOAA–CIRES–DOE Twentieth Century Reanalysis (20CR), and (d) the combined EN4–OAFlux dataset. The transparent shading in the top panels of (d) indicates the combined EN4-OAFlux uncertainty. All results are based on the 1980–2017 period.

the correlation at positive lags (i.e., Q_s *lags* SST). In the case of Fig. 13a, the correlation at negative lags exceeds the correlation at positive lags and hence $\tilde{Q}_s = \overline{Q_s'(\partial T'/\partial t)} > 0$. That is, Q_s contributes to SST variability because Q_s is positively correlated with the temperature tendencies $\partial T/\partial t$.

Importantly, the correlations between ocean heat transport and the SSTs are *also* positive when the transport leads SSTs (Fig. 13b), which suggests that ocean dynamics enhances temperature anomalies and hence drive SST variability in the unfiltered data. As is the case with the surface heat fluxes, the results inferred from lag correlations are consistent with the results derived from our Eq. (4); that is, $\tilde{Q}_o$ is positive since the transport Q_o is positively correlated with the temperature tendencies (i.e., the change in the correlation across lag zero has the same sign as the case for Q_s). Importantly, the positive contributions of ocean dynamics to SST variance could not have been unequivocally inferred from the lag correlations between surface heat fluxes and SSTs alone.

The results for low-pass filtered data (right column) are more nuanced. In this case, the correlations between Q_s and the SSTs are negative when the fluxes lead the SST field (Fig. 13c); that is, the surface heat fluxes are out of the ocean prior to the peak in the SST field. The sign of the correlations suggests that Q_s damps SST anomalies, and thus that ocean heat transport must play an essential role in driving the anomalies. The positive correlations between Q_o and the SSTs at negative lags appear to support this conclusion (Fig. 13d).

At first glance, the signs of the correlations at negative lags in Figs. 13c and 13d appear inconsistent with the results derived from Eq. (4). As noted above, previous research has interpreted the signs of the correlations to indicate that 1) the surface heat fluxes damp the positive SST anomalies at negative lags while 2) ocean heat transport enhances the SST anomalies. In contrast, our results suggest that on time scales longer than 5 years 1) the surface heat fluxes *drive* SST variability and 2) ocean heat transport *suppresses* SST variability. This apparent contradiction stems from the fact that the surface heat flux contribution to the SST variance $\tilde{Q}_s$ is a function not of the lag relationships between Q_s and the temperature, but of the covariance between Q_s and the temperature tendency, as shown by (6). Thus, as previously discussed, it is the change in the correlation between Q_s and SST across lag zero that determines the contribution of the surface heat fluxes to the temperature variance. In the case of Fig. 13c, the surface heat fluxes are negative (out of the ocean mixed layer) during periods preceding the SST anomaly, but they are *even more negative* after the peak in the SST anomaly. In this case, the sign of the change in the correlation across lag zero is the same as for the unfiltered case (Fig. 13a) and hence Q_s increases the low-frequency temperature variance.

Likewise, the ocean heat transport anomalies are positive (into the ocean mixed layer) during periods preceding the SST anomaly, but are *even more positive* after the peak in the SST anomaly. The change in the correlation across lag zero for Q_o is therefore opposite of that for Q_s (Fig. 13c) and hence Q_o reduces the low-frequency temperature variance.

Why do ocean dynamics suppress SST variance on multiannual time scales? To answer this, we revisit Fig. 9, which shows the decomposition of ocean heat transport contribution into its diffusive (Fig. 9b) and advective (Fig. 9c) components. Importantly, Fig. 9 reveals that 1) advective ocean processes contribute to multiannual SST variance $[\overline{Q_{o,\mathrm{adv}}'(\partial T'/\partial t)} > 0]$ but that 2) diffusive ocean processes suppress multiannual SST variance $[\overline{Q_{o,\mathrm{dif}}'(\partial T'/\partial t)} < 0]$. Thus, as the time scale of the mixed layer variability increases, it appears that the negative contribution from diffusion becomes increasingly large and—over certain regions of the ocean—overwhelms the positive contribution from advection. For example, in the boxed midlatitude region shown in Fig. 12, the contribution to 5-yr low-pass filtered temperature variance from advection $\tilde{Q}_{o,\mathrm{adv}}$ is $\sim 0.07\,\mathrm{K}^2$, while the contribution from diffusion $\tilde{Q}_{o,\mathrm{dif}}$ is $\sim -0.18\,\mathrm{K}^2$.

Overall, the interpretations provided here are consistent with those in Cane et al. (2017). Cane et al. (2017) use a series of idealized models to demonstrate that the signs of the lag correlations between Q_s and SST do not unambiguously identify the relative importance of ocean dynamics. For example, it is possible for the atmosphere to dominate the forcing

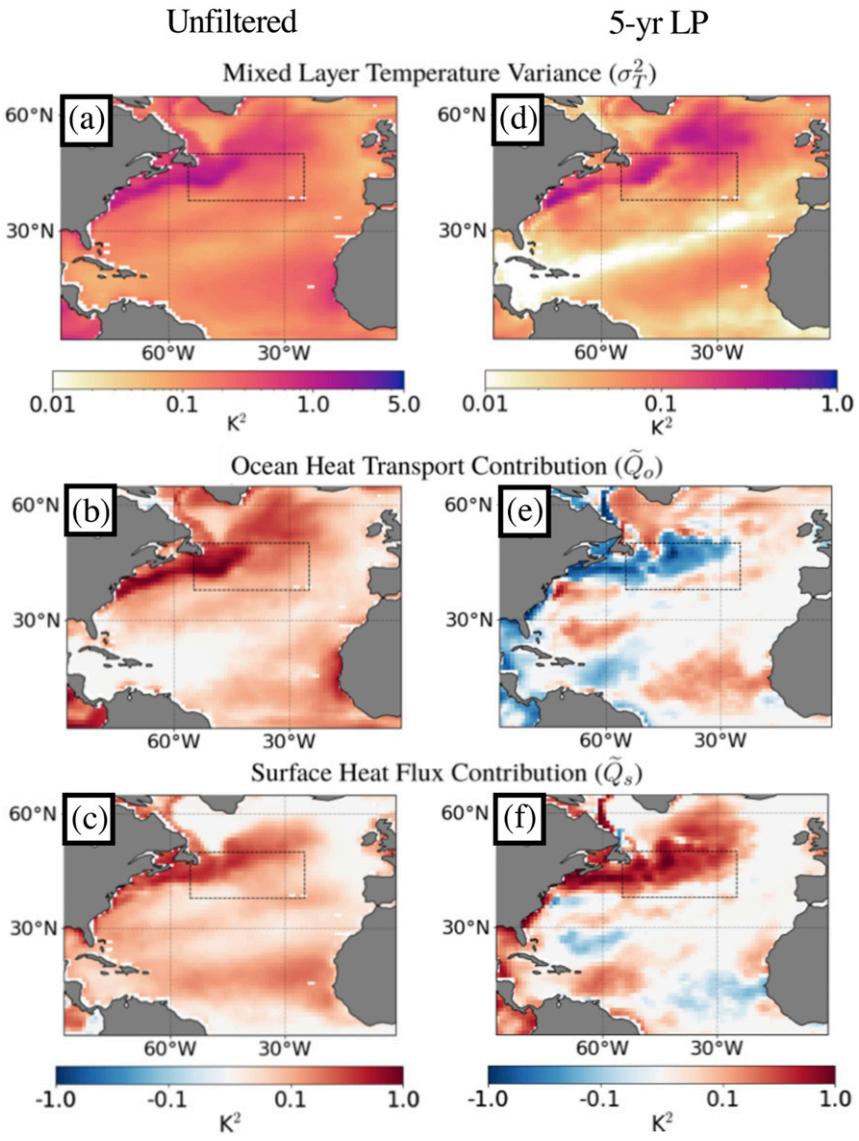

FIG. 12. As in the left column of Fig. 4, but focused on the North Atlantic sector. (a) Monthly mixed layer temperature variance from OAFlux. (b) Ocean heat transport contribution to mixed layer temperature variance derived from the indirect method using OAFlux. (c) Surface heat flux contribution to mixed layer temperature variance for OAFlux. (d)–(f) As in the left column of Fig. 8, but for 5-yr low-pass filtered data.

of SSTs but for the correlations between Q_s and SST to be negative at low frequencies, which suggests that the surface fluxes are damping low-frequency SST variability. This occurs in simple models as long as there is at least some amount of stochastic forcing from ocean dynamics, and is a consequence of quasi-equilibrium in the surface heat balance at low-frequency time scales.

Finally, we note that a key advantage of our approach is that it directly relates the variance in SSTs to the variances of the fluxes [Eqs. (4c) and (4d)]. As such, the increasingly small contributions of ocean dynamics to SST variance at lower frequencies indicates that—as the time scale increases—the variance of the ocean heat transport is decreasing more rapidly than the variance of the surface fluxes. This is depicted in Fig. 14, which shows the log ratios of the variances in Q_s to the variances in Q_o for both unfiltered and 5-yr low-pass filtered data. Clearly, the variability of the surface heat fluxes exceeds the variability of ocean heat transport in the boxed midlatitude region on longer time scales. We view Fig. 14 as compelling evidence that ocean heat transport plays a decreasingly important role in driving SST variance at multiannual time scales.

In summary, the diagnostic equation for temperature variance used here provides important insights into the relative roles of the surface heat fluxes and ocean dynamics in driving

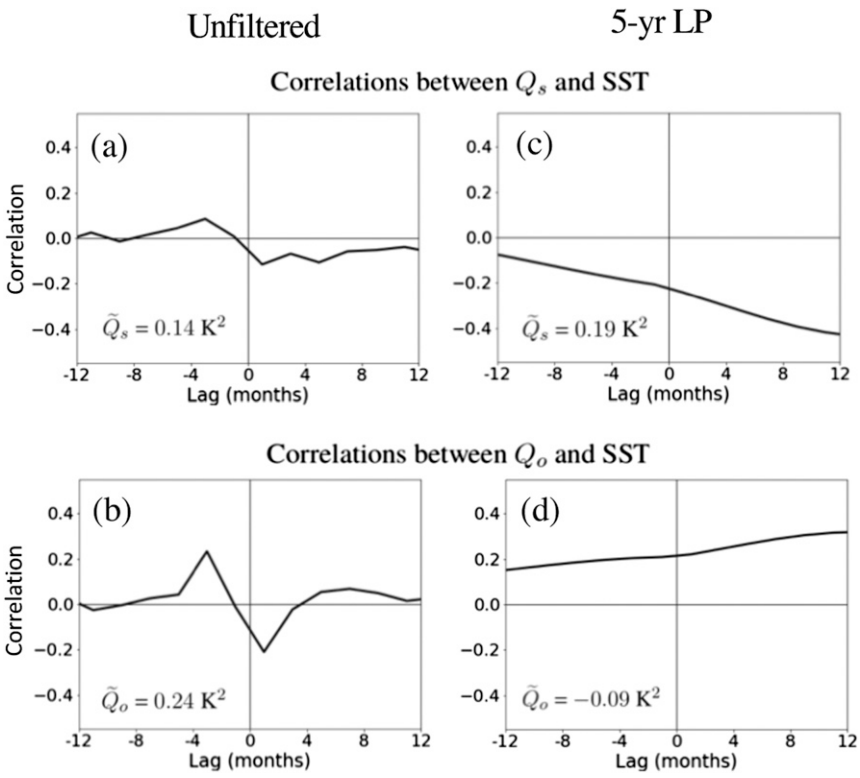

FIG. 13. (a) Lag correlations between the surface heat fluxes Q_s and SSTs for unfiltered monthly data averaged over the boxed midlatitude region (38°–50°N, 15°–55°W) shown in Fig. 12. (b) As in (a), but for lag correlations between the ocean heat transport Q_o and SSTs. (c),(d) As (a) and (b), but for 5-yr low-pass (LP) filtered data. Negative lags correspond to periods when the surface fluxes and ocean heat transport lead SSTs. The signs of Q_s and Q_o are such that positive values are into the local mixed layer. The contributions from the surface heat fluxes and ocean heat transport to the mixed layer temperature variance (i.e., $\tilde{Q}_s$ and $\tilde{Q}_o$) averaged over the boxed midlatitude region are shown in the bottom left of each panel.

mixed layer temperature variance that cannot be readily deduced from the sign of the lag correlation between Q_s and the SSTs. We have shown that the sign of the correlations between Q_s and the SSTs when the fluxes lead the SSTs does not determine the role of ocean dynamics in mixed layer temperature variance (Fig. 13). In particular, we argue that it is the change in the lag correlations about lag zero that indicates the contributions of different processes to the temperature variance, not the absolute sign of the correlations. This is most relevant on longer time scales, where the change in the correlation across lag zero is small and hence may be easily overlooked.

5. Concluding remarks

The results in this study add to an increasing body of literature that explores the role of ocean heat transport in driving SST variability. The primary novel aspects of the analyses are that 1) we provide a global survey of ocean heat transport using two distinct but complementary methodological approaches, one in which ocean heat transport is calculated directly from a state-of-the-art ocean state estimate (ECCO) and another in which it is calculated indirectly from observations; 2) we explore the resulting contributions of ocean heat transport to SST variability using a diagnostic rather than prognostic equation for the temperature variance; and 3) we probe the roles of ocean heat transport as a function of time scale across the globe in both the observations and the ECCO ocean state estimate.

The results provide novel quantitative estimates of the role of ocean dynamics in driving SST variance across the globe. Consistent with previous studies, they indicate that the largest contributions of ocean dynamics to mixed layer—and thus sea surface—temperature variability are found in the western boundary currents and their eastward extensions, the Antarctic Circumpolar Current, and the equatorial regions (e.g., Bishop et al. 2017; Roberts et al. 2017; Small et al. 2020). To leading order, the results based on the observations and the ECCO ocean state estimate yield similar spatial patterns throughout the global oceans. However, they also indicate important discrepancies in amplitude: In general, the contributions of ocean heat transport to temperature variance estimated indirectly from observations are twice as large as those estimated directly

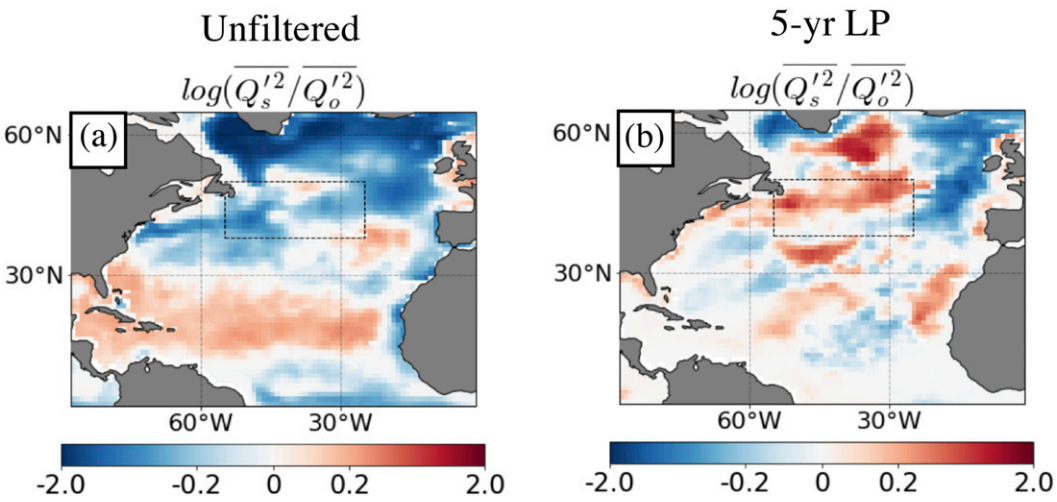

FIG. 14. (a) Log ratio of the variances of the surface heat fluxes Q_s to the variances of ocean heat transport Q_o in the North Atlantic derived from the indirect method using monthly OAFlux data. (b) As in (a), but for 5-yr low-pass filtered data.

using the ocean state estimate. The reasons for the differences in amplitude may arise from the representation of mesoscale ocean processes in the 1° ECCO product but this remains to be explored in future work.

A key result of the current study is that ocean dynamics generally play an increasingly *small* role in mixed layer temperature variability at the low-frequency time scales that are resolvable in the ECCO and OAFlux products (the records span 1992–2015 and 1980–2017, respectively). The signature of decreasing fractional contributions from ocean dynamics to mixed layer temperature variance is most clear in the Northern Hemisphere oceans, and is reproducible in a number of atmospheric reanalyses spanning 1980–2017. The decreases in the ocean dynamical contributions to mixed layer temperature variability on multiannual time scales are sufficiently large that they extend to the global average: In the case of the observations, ocean heat transport accounts for ~65% of the globally integrated variance in mixed layer temperatures on time scales of a month and longer, but only ~30% of the globally integrated variance on time scales longer than about four years. The results challenge the notion that ocean dynamics are increasingly important for SST variability at increasingly low frequencies (e.g., Bjerknes 1964; Gulev et al. 2013; Buckley et al. 2014; O'Reilly et al. 2016) and they support the hypothesis that observed low-frequency variability in the North Atlantic can be explained on the basis of stochastic processes with only a weak contribution from ocean dynamics (e.g., Clement et al. 2015; Cane et al. 2017). As discussed in section 4, the time scale–dependent contributions of ocean heat transport to mixed layer temperature variability revealed here cannot be readily inferred from the sign of the lag correlation between the surface heat fluxes and the SSTs.

Another key result is that over large regions of the Northern Hemisphere oceans, ocean dynamics act to reduce the variance of the SST field on time scales longer than a few years. Analyses of the ECCO product suggest that the suppression of SST variance arises from ocean diffusive processes: Advective ocean process contribute to SST variability across a range of time scales, but their contributions are overwhelmed by diffusion as the time scale of the SST variability increases. These results are consistent with a recent study by Murphy et al. (2020, manuscript submitted to *J. Climate*), who found weaker Atlantic multidecadal SST variability in a fully coupled GCM (CESM) relative to a slab-ocean configuration of the model. It would be interesting to explore the dependence of the results shown here on the amplitude of the convective processes and parameterized isopycnal mixing that comprise the diffusive term, as well as the spatial resolution of the ocean model.

The results shown here are derived from analyses of data extending back to 1980 (OAFlux) and 1992 (ECCO). We are hesitant to make inferences on the role of the ocean in climate variability over a longer period of record by applying a similar analysis procedure to sea surface temperatures and surface fluxes derived from, say, the 20CR product. The sea surface temperature and surface flux observations required to make such inferences are increasingly sparse and exhibit notable biases prior to ~1970 (e.g., Kent et al. 2017; Davis et al. 2019). The findings revealed here thus highlight the critical importance of continued high-quality observations of the upper ocean for understanding the role of the ocean in multidecadal climate variability.

Acknowledgments. CP was supported by the NASA Earth and Space Science Fellowship 80NSSC18K1345 and partially supported by the NSF Climate and Large-Scale Dynamics program. DWJT is supported by the NSF Climate and Large-Scale Dynamics program. We thank Laure Zanna and two anonymous reviewers for their helpful comments on the manuscript.

Data availability statement. All data are freely accessible online: OAFlux (http://oaflux.whoi.edu/), ECCO (https://ecco.jpl.nasa.gov/),

MERRA-2 reanalysis (https://gmao.gsfc.nasa.gov/reanalysis/MERRA-2/), ERA5 reanalysis (https://www.ecmwf.int/en/forecasts/datasets/reanalysis-datasets/era5), NOAA-CIRES-DOE Twentieth Century Reanalysis (https://psl.noaa.gov/data/gridded/data.20thC_ReanV3.html), and gridded analyses of ocean temperatures from the EN4 database (https://www.metoffice.gov.uk/hadobs/en4/).

APPENDIX A

Derivation of the Diagnostic Equation for Mixed Layer Temperature Variance and Uncertainty Contributions

To derive the diagnostic equation for monthly mixed layer temperature variance, i.e., Eq. (4), we start with the monthly mixed layer energy budget:

$$C_o \frac{\partial T}{\partial t} = Q_s + Q_o. \tag{A1}$$

Here, C_o is the heat capacity of the ocean mixed layer (i.e., $C_o = c_p \rho h$, where h is the ocean mixed layer depth), T is the monthly mean mixed layer temperature, Q_s is the net surface heat flux (sum of latent, sensible, and radiative heat fluxes), and Q_o is the heat convergence due to ocean dynamics, including wind-driven Ekman currents and vertical mixing. Since we are interested in understanding the processes that drive temperature anomalies, we expand each of C_o, T, Q_s, and Q_o into the sum of a climatological mean (denoted by overbars) and the departure from the mean (denoted by primes). As discussed in section 2, we also remove both the linear trend and seasonal cycle from the anomalies in C_o, T, Q_s, and Q_o. Inserting the above yields the following equation for the temperature anomalies:

$$\overline{C}_o \frac{\partial T'}{\partial t} = Q_s' + Q_o'. \tag{A2}$$

To form an equation involving the mixed layer temperature variance [i.e., $T'(t)^2$] we take the finite centered difference of the temperature tendency term in (A2), square both sides, and then average over time:

$$\frac{\overline{C}_o^2}{2\Delta t^2}\left[\overline{T'(t)^2} - \overline{T'(t+\Delta t)T'(t-\Delta t)}\right] \approx \overline{(Q_s' + Q_o')^2}, \tag{A3}$$

where Δt is the sampling period (i.e., one month). Denoting $\overline{T'(t)^2}$ as σ_T^2 and using $\overline{T'(t+\Delta t)T'(t-\Delta t)} = \overline{T'(t)T'(t-2\Delta t)} = r_2\overline{T'(t)^2}$, where r_2 is the lag-2 autocorrelation of the mixed layer temperature, we can rewrite (A3) as

$$\sigma_T^2 \approx \frac{2\Delta t^2}{\overline{C}_o^2(1-r_2)}\overline{(Q_s' + Q_o')(Q_s' + Q_o')}. \tag{A4}$$

Note that (A4) is analogous to Eq. (6) from Yu and Boer (2006).

Equation (4) that is derived in the main text is formed by using the mixed layer energy budget, (A2), to substitute the temperature tendency for one of the $Q_o' + Q_o'$ terms in (A4), and defining $\alpha = 2\Delta t^2/[\overline{C}_o(1-r_2)]$:

$$\sigma_T^2 \approx \alpha\left(\overline{\frac{\partial T'}{\partial t}Q_s'} + \overline{\frac{\partial T'}{\partial t}Q_o'}\right). \tag{A5}$$

The above is analogous to the "fraction of variance" (FOV) metric used by Buckley et al. (2014) and Roberts et al. (2017) to understand the drivers of upper-ocean heat content variability, $H = \rho c_p \overline{h} T$. Buckley et al. (2014) express the fraction of variance $\partial H/\partial t$ that is explained by Q_o, which we denote as FOV [$(\partial H/\partial t)$, Q_o], as the following:

$$\mathrm{FOV}\left(\frac{\partial H}{\partial t}, Q_o\right) = \frac{\overline{Q_o'^2} + \overline{2Q_o'Q_s'}}{\overline{\left(\frac{\partial H'}{\partial t}\right)^2}}. \tag{A6}$$

Here, we define the ocean contribution to the temperature variance as follows:

$$\tilde{Q}_o = \alpha\overline{\frac{\partial T'}{\partial t}Q_o'} = \frac{\alpha}{\overline{C}_o}(\overline{Q_o'^2} + \overline{Q_s'Q_o'}). \tag{A7}$$

Thus, both (A6) and (A7) relate to the sum of the variance of Q_o and the covariance between Q_o and Q_s. The main justification for using a single covariance term in our definition of the Q_o contribution (i.e., we have $\overline{Q_s'Q_o'}$ instead of $\overline{2Q_s'Q_o'}$) is to enable the contributions to sum to the total temperature variance (i.e., $\sigma_T^2 = \tilde{Q}_o + \tilde{Q}_s$). However, note that the covariance terms contribute equally to the surface heat flux and ocean dynamical contributions, and thus are not essential to understanding the relative contributions of Q_s and Q_o to temperature variance.

To quantify the contributions of observational error to the mixed layer temperature variance (as shown in Figs. 10a–c, B1a, and B2a), we start with

$$\tilde{Q}_s = \alpha\overline{\frac{\partial T'}{\partial t}Q_s'} = \alpha\overline{\left(\frac{\partial T'}{\partial t} \pm \varepsilon_{\frac{\partial T}{\partial t}}\right)(Q_s' \pm \varepsilon_{Q_s})}, \tag{A8}$$

where $\varepsilon_{(\partial T/\partial t)}$ and ε_{Q_s} are the observational estimates of uncertainty in the temperature tendency and surface heat fluxes, respectively. Using $\varepsilon_{(\partial T/\partial t)} \approx \varepsilon_T/\Delta t$ where ε_T is the uncertainty in the mixed layer temperature and expanding the RHS of (A8) yields

$$\tilde{Q}_s = \alpha\overline{\frac{\partial T'}{\partial t}Q_s'} \pm \overline{\frac{\partial T'}{\partial t}\varepsilon_{Q_s}} \pm \overline{Q_s'\frac{\varepsilon_T}{\Delta t}} \pm \overline{\varepsilon_{Q_s}\frac{\varepsilon_T}{\Delta t}}. \tag{A9}$$

The error in the surface heat flux contribution is then defined as

$$\varepsilon_{\tilde{Q}_s} = \overline{\frac{\partial T'}{\partial t}\varepsilon_{Q_s}} + \overline{Q_s'\frac{\varepsilon_T}{\Delta t}} + \overline{\varepsilon_{Q_s}\frac{\varepsilon_T}{\Delta t}}. \tag{A10}$$

The uncertainty in the ocean heat transport contribution is estimated from the error in the temperature variance $\varepsilon_{\sigma_T^2}$ and the error in the surface heat flux contribution using the following relation:

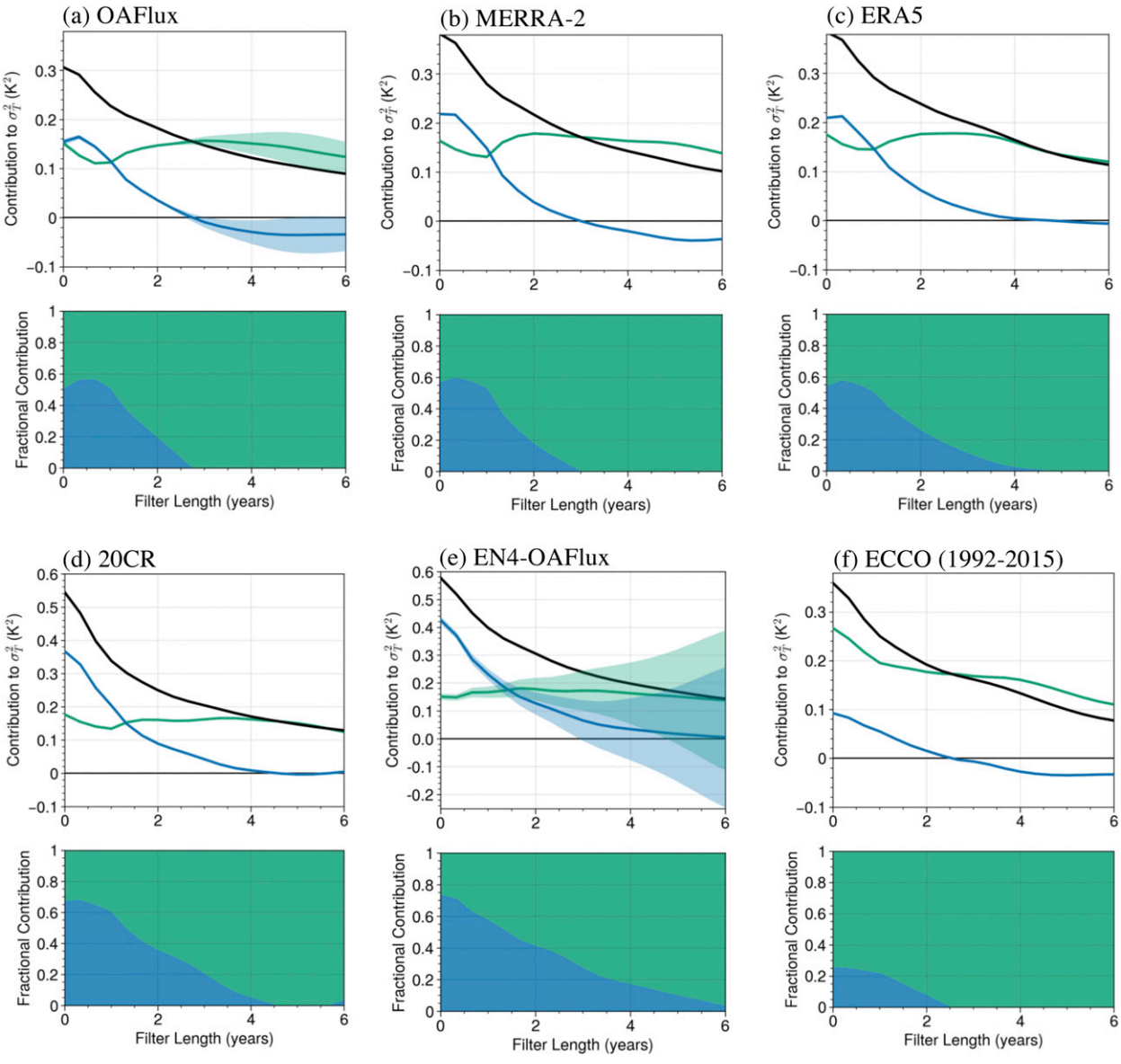

FIG. B1. (a)–(f) As in Figs. 10b, 10f, and 11a–d, but for results averaged over the North Pacific sector (defined as 20°–60°N, 120°–270°E). Results in (a)–(e) are based on the period of record 1980–2017. Results in (f) are based on the ECCO period of record 1992–2015.

$$\varepsilon_{\bar{Q}_o} = \varepsilon_{\bar{Q}_s} + \varepsilon_{\sigma_T^2}. \tag{A11}$$

This is consistent with the fact that the indirect estimate of Q_o is calculated from the observed SSTs and surface heat fluxes as a residual in the mixed layer energy budget. Note that the error in the mixed layer temperature variance is found from

$$\sigma_T^2 = \overline{(T' \pm \varepsilon_T)^2} = \overline{T'^2} \pm 2\overline{T'\varepsilon_T} + \overline{\varepsilon_T^2} \tag{A12}$$

so that

$$\varepsilon_{\sigma_T^2} = 2\overline{T'\varepsilon_T} + \overline{\varepsilon_T^2}. \tag{A13}$$

APPENDIX B

Time Scale Dependency of the Contributions to Mixed Layer Temperature Variance for the North Atlantic and North Pacific

Figures B1 and B2 show the spatially averaged contributions from the surface heat fluxes and the ocean heat transport as a function of low-pass filter length as in Figs. 10 and 11, except

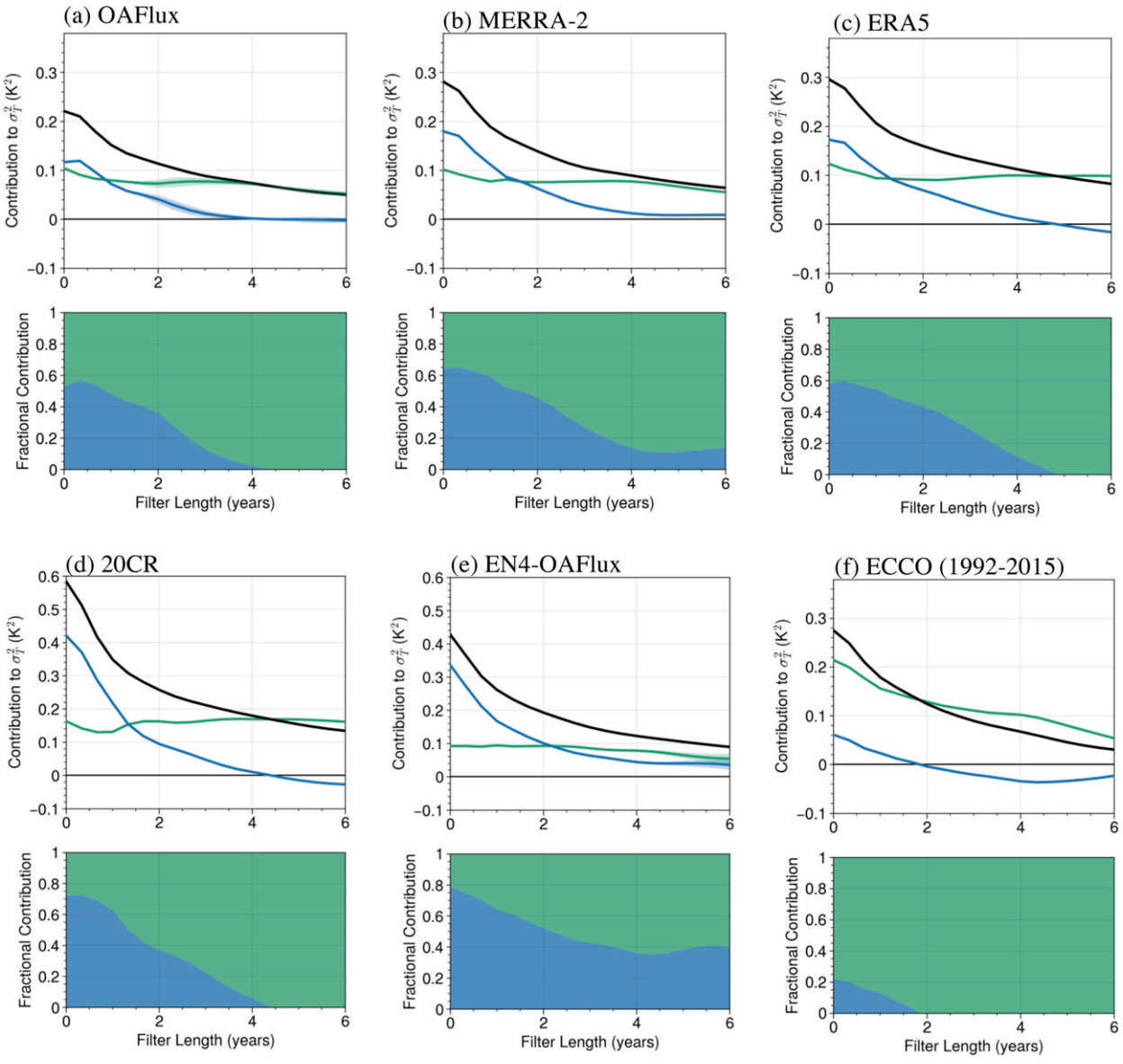

FIG. B2. As in Figs. 10b, 10f, and 11a–d, but for results averaged over the North Atlantic sector (defined as 20°–60°N, 0°–90°W). Results in (a)–(e) are based on the period of record 1980–2017. Results in (f) are based on the ECCO period of record 1992–2015.

for the North Atlantic and North Pacific basins. Figure B1 shows results for the North Pacific, and Fig. B2 shows results for the North Atlantic.

REFERENCES

Alexander, M. A., and C. Deser, 1995: A mechanism for the recurrence of wintertime midlatitude SST anomalies. *J. Phys. Oceanogr.*, **25**, 122–137, https://doi.org/10.1175/1520-0485(1995)025<0122:AMFTRO>2.0.CO;2.

——, I. Bladé, M. Newman, J. R. Lanzante, N.-C. Lau, and J. D. Scott, 2002: The atmospheric bridge: The influence of ENSO teleconnections on air–sea interaction over the global oceans. *J. Climate*, **15**, 2205–2231, https://doi.org/10.1175/1520-0442(2002)015<2205:TABTIO>2.0.CO;2.

——, and Coauthors, 2010: Extratropical air–sea interaction, sea surface temperature variability, and the Pacific decadal oscillation. *Climate Dynamics: Why Does Climate Vary*? *Geophys. Monogr.*, Vol. 189, Amer. Geophys. Union, 123–148.

Amaya, D. J., M. J. DeFlorio, A. J. Miller, and S.-P. Xie, 2017: WES feedback and the Atlantic meridional mode: Observations and CMIP5 comparisons. *Climate Dyn.*, **49**, 1665–1679, https://doi.org/10.1007/s00382-016-3411-1.

Argo, 2000: Argo float data and metadata from Global Data Assembly Centre (Argo GDAC). SEANOE, http://doi.org/10.17882/42182.

Barsugli, J. J., and D. S. Battisti, 1998: The basic effects of atmosphere–ocean thermal coupling on midlatitude variability. *J. Atmos. Sci.*, **55**, 477–493, https://doi.org/10.1175/1520-0469(1998)055<0477:TBEOAO>2.0.CO;2.

Bellomo, K., L. N. Murphy, M. A. Cane, A. C. Clement, and L. M. Polvani, 2018: Historical forcings as main drivers of the Atlantic multidecadal variability in the CESM large ensemble. *Climate Dyn.*, **50**, 3687–3698, https://doi.org/10.1007/s00382-017-3834-3.

Bishop, S. P., R. J. Small, F. O. Bryan, and R. A. Tomas, 2017: Scale dependence of midlatitude air–sea interaction. *J. Climate*, **30**, 8207–8221, https://doi.org/10.1175/JCLI-D-17-0159.1.

Bjerknes, J., 1964: Atlantic air–sea interaction. *Advances in Geophysics*, Vol. 10, Academic Press, 1–82.

Booth, B. B., N. J. Dunstone, P. R. Halloran, T. Andrews, and N. Bellouin, 2012: Aerosols implicated as a prime driver of twentieth-century North Atlantic climate variability. *Nature*, **484**, 228–232, https://doi.org/10.1038/nature10946.

Boyer, T. P., and Coauthors, 2009: World Ocean Database 2009. NOAA Atlas NESDIS 66, 216 pp.

Bryden, H. L., and S. Imawaki, 2001: Ocean heat transport. *International Geophysics*, Vol. 77, Elsevier, 455–474.

Buckley, M. W., and J. Marshall, 2016: Observations, inferences, and mechanisms of the Atlantic meridional overturning circulation: A review. *Rev. Geophys.*, **54**, 5–63, https://doi.org/10.1002/2015RG000493.

——, R. M. Ponte, G. Forget, and P. Heimbach, 2014: Low-frequency SST and upper-ocean heat content variability in the North Atlantic. *J. Climate*, **27**, 4996–5018, https://doi.org/10.1175/JCLI-D-13-00316.1.

——, ——, ——, and ——, 2015: Determining the origins of advective heat transport convergence variability in the North Atlantic. *J. Climate*, **28**, 3943–3956, https://doi.org/10.1175/JCLI-D-14-00579.1.

Cane, M. A., A. C. Clement, L. N. Murphy, and K. Bellomo, 2017: Low-pass filtering, heat flux, and Atlantic multidecadal variability. *J. Climate*, **30**, 7529–7553, https://doi.org/10.1175/JCLI-D-16-0810.1.

Cayan, D. R., 1992a: Latent and sensible heat flux anomalies over the northern oceans: Driving the sea surface temperature. *J. Phys. Oceanogr.*, **22**, 859–881, https://doi.org/10.1175/1520-0485(1992)022<0859:LASHFA>2.0.CO;2.

——, 1992b: Latent and sensible heat flux anomalies over the northern oceans: The connection to monthly atmospheric circulation. *J. Climate*, **5**, 354–369, https://doi.org/10.1175/1520-0442(1992)005<0354:LASHFA>2.0.CO;2.

Chiang, J. C., and D. J. Vimont, 2004: Analogous Pacific and Atlantic meridional modes of tropical atmosphere–ocean variability. *J. Climate*, **17**, 4143–4158, https://doi.org/10.1175/JCLI4953.1.

Clement, A., K. Bellomo, L. N. Murphy, M. A. Cane, T. Mauritsen, G. Rädel, and B. Stevens, 2015: The Atlantic multidecadal oscillation without a role for ocean circulation. *Science*, **350**, 320–324, https://doi.org/10.1126/science.aab3980.

Davis, L. L., D. W. Thompson, J. J. Kennedy, and E. C. Kent, 2019: The importance of unresolved biases in twentieth-century sea surface temperature observations. *Bull. Amer. Meteor. Soc.*, **100**, 621–629, https://doi.org/10.1175/BAMS-D-18-0104.1.

de Coëtlogon, G., and C. Frankignoul, 2003: The persistence of winter sea surface temperature in the North Atlantic. *J. Climate*, **16**, 1364–1377, https://doi.org/10.1175/1520-0442-16.9.1364.

Delworth, T. L., F. Zeng, L. Zhang, R. Zhang, G. A. Vecchi, and X. Yang, 2017: The central role of ocean dynamics in connecting the North Atlantic Oscillation to the extratropical component of the Atlantic multidecadal oscillation. *J. Climate*, **30**, 3789–3805, https://doi.org/10.1175/JCLI-D-16-0358.1.

Deser, C., M. A. Alexander, and M. S. Timlin, 2003: Understanding the persistence of sea surface temperature anomalies in midlatitudes. *J. Climate*, **16**, 57–72, https://doi.org/10.1175/1520-0442(2003)016<0057:UTPOSS>2.0.CO;2.

——, A. S. Phillips, and J. W. Hurrell, 2004: Pacific interdecadal climate variability: Linkages between the tropics and the North Pacific during boreal winter since 1900. *J. Climate*, **17**, 3109–3124, https://doi.org/10.1175/1520-0442(2004)017<3109:PICVLB>2.0.CO;2.

Dijkstra, H. A., 2008: *Dynamical Oceanography*. Springer, 407 pp.

Folland, C. K., T. N. Palmer, and D. E. Parker, 1986: Sahel rainfall and worldwide sea temperatures, 1901–85. *Nature*, **320**, 602–607, https://doi.org/10.1038/320602a0.

Forget, G., J.-M. Campin, P. Heimbach, C. N. Hill, R. M. Ponte, and C. Wunsch, 2015: ECCO version 4: An integrated framework for non-linear inverse modeling and global ocean state estimation. *Geosci. Model Dev.*, **8**, 3071–3104, https://doi.org/10.5194/gmd-8-3071-2015.

Frankignoul, C., 1985: Sea surface temperature anomalies, planetary waves, and air–sea feedback in the middle latitudes. *Rev. Geophys.*, **23**, 357–390, https://doi.org/10.1029/RG023i004p00357.

——, and K. Hasselmann, 1977: Stochastic climate models, Part II: Application to sea-surface temperature anomalies and thermocline variability. *Tellus*, **29**, 289–305, https://doi.org/10.3402/tellusa.v29i4.11362.

Frenger, I., N. Gruber, R. Knutti, and M. Münnich, 2013: Imprint of Southern Ocean eddies on winds, clouds and rainfall. *Nat. Geosci.*, **6**, 608–612, https://doi.org/10.1038/ngeo1863.

Fukumori, I., O. Wang, I. Fenty, G. Forget, P. Heimbach, and R. M. Ponte, 2017: ECCO version 4 release 3. MIT DSpace Tech. Rep., 10 pp., http://hdl.handle.net/1721.1/110380.

Gaspar, P., Y. Grégoris, and J.-M. Lefevre, 1990: A simple eddy kinetic energy model for simulations of the oceanic vertical mixing: Tests at station Papa and Long-Term Upper Ocean Study site. *J. Geophys. Res.*, **95**, 16 179–16 193, https://doi.org/10.1029/JC095iC09p16179.

Gelaro, R., and Coauthors, 2017: The Modern-Era Retrospective Analysis for Research and Applications, version 2 (MERRA-2). *J. Climate*, **30**, 5419–5454, https://doi.org/10.1175/JCLI-D-16-0758.1.

Gent, P. R., and J. C. McWilliams, 1990: Isopycnal mixing in ocean circulation models. *J. Phys. Oceanogr.*, **20**, 150–155, https://doi.org/10.1175/1520-0485(1990)020<0150:IMIOCM>2.0.CO;2.

Good, S. A., M. J. Martin, and N. A. Rayner, 2013: EN4: Quality controlled ocean temperature and salinity profiles and monthly objective analyses with uncertainty estimates. *J. Geophys. Res. Oceans*, **118**, 6704–6716, https://doi.org/10.1002/2013JC009067.

Griffies, S. M., and Coauthors, 2015: Impacts on ocean heat from transient mesoscale eddies in a hierarchy of climate models. *J. Climate*, **28**, 952–977, https://doi.org/10.1175/JCLI-D-14-00353.1.

Gulev, S. K., M. Latif, N. Keenlyside, W. Park, and K. P. Koltermann, 2013: North Atlantic Ocean control on surface heat flux on multidecadal timescales. *Nature*, **499**, 464–467, https://doi.org/10.1038/nature12268.

Hall, M. M., and H. L. Bryden, 1982: Direct estimates and mechanisms of ocean heat transport. *Deep-Sea Res.*, **29**, 339–359, https://doi.org/10.1016/0198-0149(82)90099-1.

Hartmann, D. L., 2015: *Global Physical Climatology*. Vol. 103, Newnes, 498 pp.

Hasselmann, K., 1976: Stochastic climate models part I. Theory. *Tellus*, **28**, 473–485, https://doi.org/10.1111/j.2153-3490.1976.tb00696.x.

Hersbach, H., and D. Dee, 2016: ERA5 reanalysis is in production. *ECMWF Newsletter*, No. 147, ECMWF, Reading, United

Kingdom, 7, http://www.ecmwf.int/sites/default/files/elibrary/2016/16299-newsletter-no147-spring-2016.pdf.

Jin, F.-F., 1997: An equatorial ocean recharge paradigm for ENSO. Part I: Conceptual model. *J. Atmos. Sci.*, **54**, 811–829, https://doi.org/10.1175/1520-0469(1997)054<0811:AEORPF>2.0.CO;2.

Kent, E. C., and Coauthors, 2017: A call for new approaches to quantifying biases in observations of sea surface temperature. *Bull. Amer. Meteor. Soc.*, **98**, 1601–1616, https://doi.org/10.1175/BAMS-D-15-00251.1.

Kim, W. M., S. Yeager, P. Chang, and G. Danabasoglu, 2018: Low-frequency North Atlantic climate variability in the Community Earth System Model large ensemble. *J. Climate*, **31**, 787–813, https://doi.org/10.1175/JCLI-D-17-0193.1.

Kirtman, B. P., and Coauthors, 2012: Impact of ocean model resolution on CCSM climate simulations. *Climate Dyn.*, **39**, 1303–1328, https://doi.org/10.1007/s00382-012-1500-3.

Kushnir, Y., W. Robinson, I. Bladé, N. Hall, S. Peng, and R. Sutton, 2002: Atmospheric GCM response to extratropical SST anomalies: Synthesis and evaluation. *J. Climate*, **15**, 2233–2256, https://doi.org/10.1175/1520-0442(2002)015<2233:AGRTES>2.0.CO;2.

Kwon, Y.-O., and C. Deser, 2007: North Pacific decadal variability in the Community Climate System Model version 2. *J. Climate*, **20**, 2416–2433, https://doi.org/10.1175/JCLI4103.1.

Latif, M., and T. P. Barnett, 1994: Causes of decadal climate variability over the North Pacific and North America. *Science*, **266**, 634–637, https://doi.org/10.1126/science.266.5185.634.

Ma, X., and Coauthors, 2015: Distant influence of Kuroshio eddies on North Pacific weather patterns? *Sci. Rep.*, **5**, 17785, https://doi.org/10.1038/srep17785.

——, and Coauthors, 2016: Western boundary currents regulated by interaction between ocean eddies and the atmosphere. *Nature*, **535**, 533–537, https://doi.org/10.1038/nature18640.

Mantua, N. J., S. R. Hare, Y. Zhang, J. M. Wallace, and R. C. Francis, 1997: A Pacific interdecadal climate oscillation with impacts on salmon production. *Bull. Amer. Meteor. Soc.*, **78**, 1069–1080, https://doi.org/10.1175/1520-0477(1997)078<1069:APICOW>2.0.CO;2.

McPhaden, M. J., S. E. Zebiak, and M. H. Glantz, 2006: ENSO as an integrating concept in Earth science. *Science*, **314**, 1740–1745, https://doi.org/10.1126/science.1132588.

Murphy, L. N., K. Bellomo, M. A. Cane, and A. C. Clement, 2017: The role of historical forcings in simulating the observed Atlantic multidecadal oscillation. *Geophys. Res. Lett.*, **44**, 2472–2480, https://doi.org/10.1002/2016GL071337.

Newman, M., G. P. Compo, and M. A. Alexander, 2003: ENSO-forced variability of the Pacific decadal oscillation. *J. Climate*, **16**, 3853–3857, https://doi.org/10.1175/1520-0442(2003)016<3853:EVOTPD>2.0.CO;2.

——, and Coauthors, 2016: The Pacific decadal oscillation, revisited. *J. Climate*, **29**, 4399–4427, https://doi.org/10.1175/JCLI-D-15-0508.1.

O'Reilly, C. H., and L. Zanna, 2018: The signature of oceanic processes in decadal extratropical SST anomalies. *Geophys. Res. Lett.*, **45**, 7719–7730, https://doi.org/10.1029/2018GL079077.

——, M. Huber, T. Woollings, and L. Zanna, 2016: The signature of low-frequency oceanic forcing in the Atlantic Multidecadal Oscillation. *Geophys. Res. Lett.*, **43**, 2810–2818, https://doi.org/10.1002/2016GL067925.

Pedlosky, J., 2013: *Ocean Circulation Theory*. Springer, 456 pp.

Philander, S. G. H., 1983: El Niño Southern Oscillation phenomena. *Nature*, **302**, 295–301, https://doi.org/10.1038/302295a0.

Putrasahan, D., I. Kamenkovich, M. Le Hénaff, and B. Kirtman, 2017: Importance of ocean mesoscale variability for air–sea interactions in the Gulf of Mexico. *Geophys. Res. Lett.*, **44**, 6352–6362, https://doi.org/10.1002/2017GL072884.

Qiu, B., N. Schneider, and S. Chen, 2007: Coupled decadal variability in the North Pacific: An observationally constrained idealized model. *J. Climate*, **20**, 3602–3620, https://doi.org/10.1175/JCLI4190.1.

Redi, M. H., 1982: Oceanic isopycnal mixing by coordinate rotation. *J. Phys. Oceanogr.*, **12**, 1154–1158, https://doi.org/10.1175/1520-0485(1982)012<1154:OIMBCR>2.0.CO;2.

Reynolds, R. W., T. M. Smith, C. Liu, D. B. Chelton, K. S. Casey, and M. G. Schlax, 2007: Daily high-resolution-blended analyses for sea surface temperature. *J. Climate*, **20**, 5473–5496, https://doi.org/10.1175/2007JCLI1824.1.

Roberts, C. D., M. D. Palmer, R. P. Allan, D. G. Desbruyeres, P. Hyder, C. Liu, and D. Smith, 2017: Surface flux and ocean heat transport convergence contributions to seasonal and interannual variations of ocean heat content. *J. Geophys. Res. Oceans*, **122**, 726–744, https://doi.org/10.1002/2016JC012278.

Saravanan, R., and P. Chang, 2019: Midlatitude mesoscale ocean–atmosphere interaction and its relevance to S2S prediction. *Sub-Seasonal to Seasonal Prediction*, Elsevier, 183–200.

Schlesinger, M. E., and N. Ramankutty, 1994: An oscillation in the global climate system of period 65–70 years. *Nature*, **367**, 723–726, https://doi.org/10.1038/367723a0.

Schneider, N., A. J. Miller, and D. W. Pierce, 2002: Anatomy of North Pacific decadal variability. *J. Climate*, **15**, 586–605, https://doi.org/10.1175/1520-0442(2002)015<0586:AONPDV>2.0.CO;2.

Siqueira, L., and B. P. Kirtman, 2016: Atlantic near-term climate variability and the role of a resolved Gulf Stream. *Geophys. Res. Lett.*, **43**, 3964–3972, https://doi.org/10.1002/2016GL068694.

Slivinski, L. C., andCoauthors, 2019: Towards a more reliable historical reanalysis: Improvements for version 3 of the Twentieth Century Reanalysis system. *Quart. J. Roy. Meteor. Soc.*, **145**, 2876–2908, https://doi.org/10.1002/qj.3598.

Small, R. J., and Coauthors, 2008: Air–sea interaction over ocean fronts and eddies. *Dyn. Atmos. Oceans*, **45**, 274–319, https://doi.org/10.1016/j.dynatmoce.2008.01.001.

——, F. O. Bryan, S. P. Bishop, and R. A. Tomas, 2019: Air–sea turbulent heat fluxes in climate models and observational analyses: What drives their variability? *J. Climate*, **32**, 2397–2421, https://doi.org/10.1175/JCLI-D-18-0576.1.

——, ——, ——, S. Larson, and R. A. Tomas, 2020: What drives upper-ocean temperature variability in coupled climate models and observations? *J. Climate*, **33**, 577–596, https://doi.org/10.1175/JCLI-D-19-0295.1.

Talley, L., 1984: Meridional heat transport in the Pacific Ocean. *J. Phys. Oceanogr.*, **14**, 231–241, https://doi.org/10.1175/1520-0485(1984)014<0231:MHTITP>2.0.CO;2.

Trenberth, K. E., and J. M. Caron, 2001: Estimates of meridional atmosphere and ocean heat transports. *J. Climate*, **14**, 3433–3443, https://doi.org/10.1175/1520-0442(2001)014<3433:EOMAAO>2.0.CO;2.

U.S. National Oceanographic Data Center, 2006: Global Temperature-Salinity Profile Programme, NOAA, National Oceanographic Data Center, accessed September 2012, http://www.nodc.noaa.gov/GTSPP/.

Wills, R. C., K. C. Armour, D. S. Battisti, and D. L. Hartmann, 2019a: Ocean–atmosphere dynamical coupling fundamental to the Atlantic multidecadal oscillation. *J. Climate*, **32**, 251–272, https://doi.org/10.1175/JCLI-D-18-0269.1.

——, D. S. Battisti, C. Proistosescu, L. Thompson, D. L. Hartmann, and K. C. Armour, 2019b: Ocean circulation signatures of

North Pacific decadal variability. *Geophys. Res. Lett.*, **46**, 1690–1701, https://doi.org/10.1029/2018GL080716.

Xie, S.-P., and J. A. Carton, 2004: Tropical Atlantic variability: Patterns, mechanisms, and impacts. *Earth Climate: The Ocean–Atmosphere Interaction*, *Geophys. Monogr.*, Vol. 147, Amer. Geophys. Union, 121–142.

Yan, X., R. Zhang, and T. R. Knutson, 2018: Underestimated AMOC variability and implications for AMV and predictability in CMIP models. *Geophys. Res. Lett.*, **45**, 4319–4328, https://doi.org/10.1029/2018GL077378.

Yu, B., and G. Boer, 2006: The variance of sea surface temperature and projected changes with global warming. *Climate Dyn.*, **26**, 801–821, https://doi.org/10.1007/s00382-006-0117-9.

Yu, L., X. Jin, and R. A. Weller, 2008: Multidecade global flux datasets from the Objectively Analyzed Air–Sea Fluxes (OAFlux) project: Latent and sensible heat fluxes, ocean evaporation, and related surface meteorological variables. OAFlux Project Tech. Rep. OA-2008-01, 64 pp.

Zhang, L., and C. Wang, 2013: Multidecadal North Atlantic sea surface temperature and Atlantic meridional overturning circulation variability in CMIP5 historical simulations. *J. Geophys. Res. Oceans*, **118**, 5772–5791, https://doi.org/10.1002/jgrc.20390.

Zhang, R., 2017: On the persistence and coherence of subpolar sea surface temperature and salinity anomalies associated with the Atlantic multidecadal variability. *Geophys. Res. Lett.*, **44**, 7865–7875, https://doi.org/10.1002/2017GL074342.

——, R. Sutton, G. Danabasoglu, T. L. Delworth, W. M. Kim, J. Robson, and S. G. Yeager, 2016: Comment on ''The Atlantic multidecadal oscillation without a role for ocean circulation.'' *Science*, **352**, 1527, https://doi.org/10.1126/science.aaf1660.

——, ——, ——, Y.-O. Kwon, R. Marsh, S. G. Yeager, D. E. Amrhein, and C. M. Little, 2019: A review of the role of the Atlantic Meridional Overturning Circulation in Atlantic multidecadal variability and associated climate impacts. *Rev. Geophys.*, **57**, 316–375, https://doi.org/10.1029/2019RG000644.